REVIEW

Check for updates

Fluorescent probes for visualizing ROS-associated proteins in disease

Hui Wang,[a] Xin Wang,[a] Ping Li, [ID] *[a] Mingyan Dong,[a] Shao Q. Yao [ID] *[b] and Bo Tang [ID] *[a]

Abnormal expression of proteins, including catalytic and expression dysfunction, is directly related to the development of various diseases in living organisms. Reactive oxygen species (ROS) could regulate protein expression by redox modification or cellular signal pathway and thus influence the development of disease. Determining the expression level and activity of these ROS-associated proteins is of considerable importance in early-stage disease diagnosis and the identification of new drug targets. Fluorescence imaging technology has emerged as a powerful tool for specific *in situ* imaging of target proteins by virtue of its non-invasiveness, high sensitivity and good spatiotemporal resolution. In this review, we summarize advances made in the past decade for the design of fluorescent probes that have contributed to tracking ROS-associated proteins in disease. We envision that this review will attract significant attention from a wide range of researchers in their utilization of fluorescent probes for *in situ* investigation of pathological processes synergistically regulated by both ROS and proteins.

1. Introduction

All cells depend on preserving protein homeostasis to maintain the correct biological functions. In response to pathological stimuli, hundreds of proteins are aberrantly expressed, accompanied by abnormal changes in the activities of numerous enzymes in cells. Abundant reports have suggested

[a]*College of Chemistry, Chemical Engineering and Materials Science, Key Laboratory of Molecular and Nano Probes, Ministry of Education, Collaborative Innovation Center of Functionalized Probes for Chemical Imaging in Universities of Shandong, Institute of Biomedical Sciences, Shandong Normal University, Jinan 250014, P. R. China. E-mail: lip@sdnu.edu.cn; tangb@sdnu.edu.cn*

[b]*Department of Chemistry, National University of Singapore, Singapore 117543, Singapore. E-mail: chmyaosq@nus.edu.sg*

that neurodegenerative disorders, such as Alzheimer's disease (AD) and prion disease, share similar cellular and molecular mechanisms, including deviant protein aggregation and deposition.[1,2] The development and metastasis of cancer is also directly related to abnormal expression levels of proteins including up/down-regulated activities of enzymes.[3–5] Take cathepsins for example: many of these enzymes exhibit high proteinase activity in tumour cells and participate in angiogenesis and cell invasion.[6] The activity of matrix metalloproteinases, another class of well-known enzymes, is also elevated in many tumour cells to degrade extracellular matrix proteins and promote tumour metastasis.[7]

A series of oxygen metabolites, including superoxide anions $(O_2^{\cdot-})$, hydrogen peroxide (H_2O_2), hydroxyl radicals $(\cdot OH)$,

Hui Wang received her PhD degree from Nankai University in 2013. She is an associate professor in the College of Chemistry at Shandong Normal University. Her current research interests include design and synthesis of dual-mode fluorescent probes for enzymes and fluorescence imaging of Golgi biomarkers in disease.

Xin Wang received her PhD degree at the college of Chemistry, Chemical Engineering and Materials Science in Shandong Normal University in 2020. Her research interests are focused on two-photon fluorescence imaging of depression related active molecules in vivo.

organic peroxides and so on, collectively known as reactive oxygen species (ROS), are present in mammalian cells.[8,9] Intracellular ROS are constantly generated at low concentrations, which can regulate protein expression by redox modification or cellular signal pathways.[10,11] When cells undergo oxidative stress, amino acid residues in many susceptible proteins may be damaged by oxidative outburst. For instance, ROS can convert the side chains of certain amino acid residues (*i.e.*, Pro, Arg and Lys) into glutamic semialdehydes and aminoadipic semialdehydes by iron-catalyzed oxidation.[12] ROS also mediate the formation of 3-nitrotyrosine in proteins by nitration of tyrosine residues. These oxidative modifications might destroy the targeted protein structures and affect their functions, consequently affecting metabolism, protein folding and degradation of the false proteins. Eventually, various serious diseases may occur as a result.

Therefore, it is vitally necessary to accurately detect the expression and activity of ROS-associated proteins in disease *in vivo*. This will enable identification of damaged metabolic networks at early stages of diseases, as well as their pathogenesis, leading to acceleration of early diagnosis of major diseases and their drug development.

Although several approaches have been employed to assess the level of protein expression, such as two-dimensional electrophoresis (2-DE), immunoblotting and immunofluorescence techniques, they have severe limitations. (1) In immunoblotting and 2-DE, the protein of interest (POI) needs to be extracted from cells or tissue homogenates, which may degrade due to temperature, pH and protease, leading to inaccurate test results. (2) Immunofluorescence requires specific binding of fluorophore labelled antibodies to their antigens and measures the expression levels of proteins based on fluorescence signals. Although protein extraction is avoided in immunofluorescence, this technique can only be performed on dead cells or fixed tissue slices, which could not be implemented for noninvasive studies of cells and intact organisms. In summary, these

Ping Li received her PhD degree in 2008 from Shandong Normal University. In 1998, she joined the faculty at Shandong Normal University, where she is currently a professor of the College of Chemistry, Chemical Engineering and Materials Science. She is Taishan Distinguished Professor and the leader of the Changjiang Scholars and Innovative Research Team in University. Her research interests include synthesis and bioimaging application of fluorescent probes for biologically active molecules.

Shao Q. Yao received his PhD from Purdue University (1998) and post-doctoral training (1998–2001) from University of California, Berkeley and The Scripps Research Institute. He joined National University of Singapore (NUS) in 2001 and is currently a Full Professor at the Department of Chemistry, NUS. His current research interest is in catalomics – proteome-wide interrogation of enzymes and their associated molecules by using techniques in chemistry, biology and materials science. He is currently on the scientific advisory board of numerous international journals.

Mingyan Dong is currently pursuing a masters degree at the college of Chemistry, Chemical Engineering and Materials Science in Shandong Normal University. Her research interests are focused on two-photon fluorescence imaging of intracellular microenvironment.

Bo Tang is now a professor of chemistry at Shandong Normal University. He received his PhD degree in 1994 from Nankai University. He began his independent career as a professor of chemistry at Shandong Normal University in 1994. He obtained the National Fund for Outstanding Young Scientists in 2007, and was a Chief Scientist for the 973 Program in 2012. His research interests include the synthesis of molecular and nano probes and the application in biological imaging, green chemical production, synthesis of fluorescent materials, solar chemical conversion and storage and so on. He has contributed more than 300 journal articles, as well as 21 invited book chapters and reviews, and obtained 39 granted patents.

methods could not be applied for accurate *in situ* protein detection *in vivo*.

Recently, fluorescent probes have been widely used in conjunction with fluorescence imaging techniques to track molecular events in living cells. Fluorescence imaging is a noninvasive approach for *in situ* detection of various biomolecules.[13,14] So, by using fluorescence-based probes, the expression level and catalytic activity of ROS-associated proteins could be continuously monitored *in situ* in living cells on a real-time scale, which demonstrates broad application prospects compared with traditional methods. In this review, to provide strategies used in the design of fluorescence probes for ROS-relevant proteins and their application to the detection of disease, we summarize recently published fluorescent probes for the optical detection of ROS-associated proteins in disease. Considering proteins with and without catalytic activity, we clarify the difference between design strategies of fluorescent probes for them. Subsequently, according to different diseases, recent examples and applications of fluorescent probes for the measurement of ROS-associated proteins in the past decade will be introduced. Finally, with the aim of exploiting more powerful imaging tools in this area, we will give a perspective on further challenges and opportunities in this field.

2. Classification of proteins and probe design strategies

Proteins are major targets of ROS. Some ROS-induced protein modifications can result in unfolding or alteration of protein structure and activity. For example, ROS-mediated *S*-gluta-thionylation, nitrosation, and carbonylation play significant roles in the modulation of protein function in cells. The overall biology of oxidative protein modifications however remains complicated and undefined. Thus, development of fluorescent probes for detection of ROS-associated proteins could be quite beneficial for a better understanding of oxidative-damaged proteins in various diseases. Typically, proteins can be broadly divided into two groups, one with catalytic activity (the so-called enzymes) and the other without catalytic activity. According to their different characterizations, feasible strategies should be proposed for the design of their corresponding fluorescent probes.

For enzymatic activity-based fluorescent probes, the covalent bond is cleaved/formed or the functional group transformed into a new group under specific enzyme-catalysed conditions. These reactions will change the optical properties of the probe, such as different fluorescence intensities or emission wavelengths, and consequently report the activity of the enzyme.[15] However, the chemical structures of the probes would not be altered when they encounter proteins without catalytic activity, but the microenvironmental changes strongly affect the photophysical properties or the aggregated states of the probes. These alterations are accompanied by changes in the fluorescence intensity of the probe, leading to detection and monitoring of the protein expression level.

2.1. Design strategies of fluorescent probes for proteins with catalytic activity

Most ROS-associated enzymes could be classified into different classes according to the different chemical reactions they catalyse, such as oxido-reductases, hydrolases, and transferases. Oxido-reductases can catalyse the transfer of electrons between metabolites in order to maintain redox homeostasis. Numerous oxido-reductases exhibit direct relationships with various human diseases. For instance, monoamine oxidases are over-expressed in Alzheimer's disease. In addition, nitroreductases play essential roles in tumour metastasis. Hydrolases, including lipases, nucleosidases, and peptidases, are a class of enzymes that catalyse the hydrolysis of some chemical bonds, and are widely used as disease biomarkers. The activities of caspases, metallomembrane proteases, and aminopeptidases, all of which are sub-classes of peptidases, are common indicators of cancer. Transferases can transfer specific functional groups from the donor to acceptor substances, and among them, glycosyl transferases are involved in transferring mono-saccharides in metabolisms.

Since enzymes show high specificity toward substrates in catalytic reactions, specific chemical structures or chemical bonds could be recognized. For example, glucosidases just hydrolyse the glucose-formed glucosidic bond. On the basis of enzymes' features, various fluorescent probes have been synthesized for the assessment of different catalytic activities in numerous biological processes in the past decade, especially those relevant to major human diseases.

How to regulate optical properties of a fluorescent probe before and after it is catalysed by the target enzyme is the key factor in the probe design. In general, fluorescence properties of the probes are tuned by intermolecular charge transfer (ICT), intermolecular photoinduced electron transfer (PeT), fluorescence resonance energy transfer (FRET), and so on (Fig. 1). When enzymatic reactions cause the cleavage of covalent bonds or the alteration of functional groups in the probes, fluorescence signals emitted by the probes can be subsequently changed, leading to eventual qualitative or quantitative detection of the target enzymes.

2.2. Design strategies of fluorescent probes for proteins without catalytic activity

Numerous proteins without catalytic activity participate in cellular metabolism, and are also closely associated with various diseases caused by aggregation of proteins such as β-amyloid (Aβ) and tau. The expression levels of these proteins fluctuate during the course of pathology development, and thus have emerged as potential diagnostic biomarkers of these diseases. Since these proteins do not possess any catalytic activity and cannot catalyse the cleavage or formation of covalent bonds, they can't alter the molecular structures of a fluorescent probe. Thus, to image these proteins, the design of the corresponding fluorescent probes requires very different strategies from those for the enzymatic probes. Fluorescent probes based on the aggregation-induced emission (AIE) mechanism
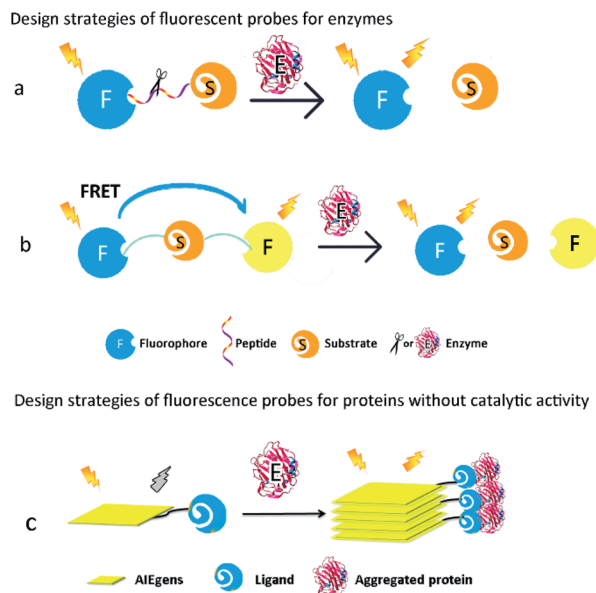
Design strategies of fluorescent probes for enzymes

Design strategies of fluorescence probes for proteins without catalytic activity

Fig. 1 Design strategies of fluorescent probes for proteins with or without catalytic activity.

and environmental-sensitive strategies have been developed in the past decade.[16,17]

AIE-based fluorescent probes are composed of two parts, namely, AIE luminogens (AIEgens) and a specific ligand of target proteins (Fig. 1c). The connection between AIEgens and the ligand is classified into either a covalent bond or non-covalent binding. The latter usually connects AIEgens and the ligand by hydrogen bonding, ionic bonding, and hydrophobic interaction. A ligand with high affinity and specificity forces AIEgens of the fluorescent probes to accumulate at the proximity of aggregated proteins. AIEgens are nonemissive in the dispersed state as earlier mentioned, due to their ability to consume the excited-state energy through intramolecular motion upon being photo-excited. In their aggregated state on the other hand, AIEgens emit intense fluorescence because the intramolecular motion is spatially restricted.[18] Therefore, AIE-based fluorescent probes can afford useful imaging information of aggregated peptides or proteins, especially those commonly found in neurodegenerative diseases, such as Aβ and tau.[19,20]

For proteins whose expression levels are clearly affected by their surrounding environment, such as polarity and viscosity, environment-sensitive fluorescent probes are often used to detect them.[21] These probes contain either a donor–acceptor or donor–acceptor–donor, which is connected by a conjugated π-bridge. Depending on whether intramolecular rotation is limited, the probe's coplanarity differs in the excited state upon successful binding to the target protein. Better coplanarity of the fluorescent probe causes a strong fluorescence change or red-shift of the emission wavelength, which can be effectively correlated with the expression level of the target protein.[22] Because the aggregation of Aβ and tau dramatically alters these proteins' surrounding polarity and viscosity in cells, many environment-sensitive fluorescent probes, designed for imaging

of these proteins based on changes in their intramolecular rotation, have been reported in the past decade.[23–25]

3. Fluorescent probes for ROS-associated proteins in diseases

Many post-translational modifications of proteins could be controlled or caused by ROS. For instance, the sulfhydryl group in cysteine residues of proteins can be oxidized to form an intramolecular disulphide bridge by H_2O_2 or sulphur reactive radicals. Various diseases, including cancer (*e.g.*, hepatic carcinoma), cerebral disease (*e.g.*, depression), cardiovascular diseases (*e.g.*, ischemia reperfusion), fibrotic diseases (*e.g.*, pulmonary fibrosis), and inflammations (*e.g.*, arthritis), have been reported to possess direct relevance to the expression level or the activities of critical ROS-associated proteins.[26]

3.1. Cancer

ROS can promote tumour development and progression in various types of cancers. In cancer cells, high levels of ROS are generated as a result of increased enzymatic activities in oxidases, cyclooxygenases, and lipoxygenases. The excess ROS overwhelms the antioxidant systems (*e.g.*, coenzyme Q, ferritin, glutathione, superoxide dismutase, thioredoxins and peroxidases), leading to oxidative stress.[27,28] In order to maintain the delicate balance of intracellular ROS levels, the expression level of antioxidant proteins (such as thioredoxins and peroxidases) in tumour cells is elevated. Moreover, many proteins involved in cell proliferation, differentiation, biomacromolecule synthesis, tissue invasion and metastasis, are also known to be ROS-sensitive in various cancers.[29]

3.1.1 Fluorescent probes for caspases. Apoptosis is a type of programmed cell death, which blocks metastatic dissemination by killing tumour cells. Caspases are a family of cysteine-dependent aspartate-specific proteases, which can cleave the carboxy-terminal side of aspartic acid residues in peptides and proteins.[30] The caspases are generally divided into two classes: the initiator caspases (caspase-2, -8, -9 and -10) and the downstream effector caspases (caspases-3, -6 and -7) in mammals.[31,32] During apoptosis response, caspases are the pivotal enzymes that are activated.[33] The accumulation of ROS often induces caspase-dependent apoptosis in cancer cells.[34] For example, methyl jasmonate induces apoptosis in human lung adenocarcinoma cells *via* activating caspase-9 and caspase-3 by over-generation of intracellular H_2O_2.[35] In consideration of the fact that caspases participate in the apoptosis signalling pathway in cancers, fluorescent probes capable of assaying and imaging various caspase activities have attracted much attention in recent years.[36,37] Since caspase-3 usually acts as a biomarker of apoptosis, fluorescent probes for monitoring the activity of caspase-3 are summarized below.[38]

DEVD (Asp–Glu–Val–Asp) is the most commonly used peptide substrate to be specifically hydrolyzed by caspase-3,[39] but DEVD is also the optimum substrate for caspase-7. Therefore, the fluorescence probes that are designed based on DEVD as the substrate to detect caspase-3/7 cannot selectively respond
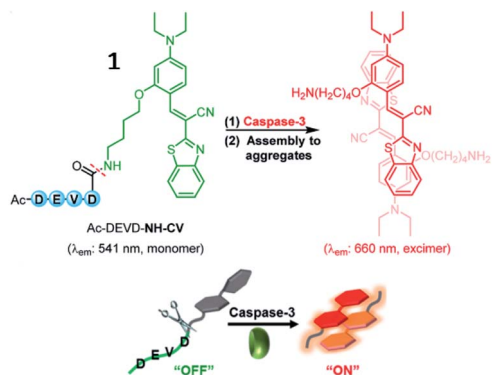
Fig. 2 Proposed turn-on sensing of probe **1** for caspase-3. Reprinted from ref. 42 with permission. Copyright 2017 American Chemical Society.

to caspase-3 or caspase-7. Nevertheless, several fluorescence probes were still developed by introducing DEVD into the probe to detect caspase-3.

Several small-molecule fluorescence probes for detection of caspases have been reported.[40,41] Kim *et al.* described a water-soluble fluorescent probe (**1**, Ac-DEVD-NH-CV) responsive to caspase-3 (Fig. 2). After being cleaved by caspase-3, the probe (**1**) was converted into hydrophobic CV-NH$_2$, which would aggregate and emit strong fluorescence. This probe was an attractive tool to study caspase-3 *in vitro* and *in vivo*.[42]

Jiang *et al.* developed a small-molecule probe (**2**) for fluorescence imaging of caspase-8 activity through a thiol-ene click reaction (Fig. 3).[43] Upon reaction with caspase-8, the probe (**2**) was cleaved at the peptide bond between cysteine and the caspase-8-specific substrate, releasing the fluorophore. Due to the intramolecular hydrogen bonds, probe **2** locally aggregated and emitted bright fluorescence at 520 nm. This is the first
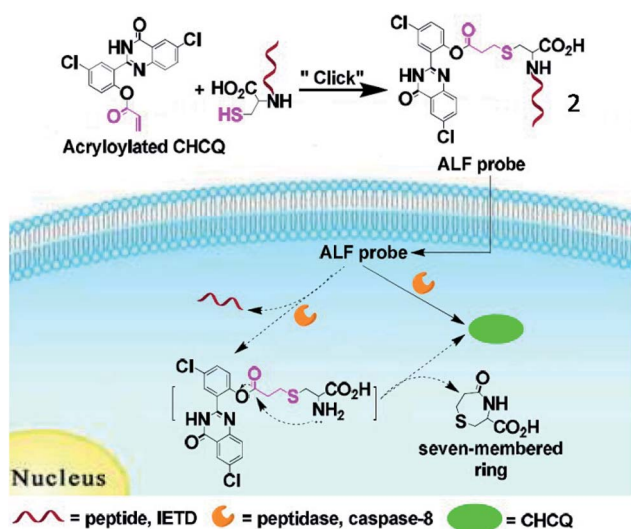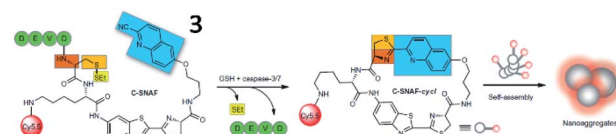
fluorescent probe based on a thiol-Michael addition click reaction for bioimaging of caspase.

Based on the cyclization reaction between free cysteine and 2-cyano-6-hydroxyquinoline (CHQ), Rao and Ye *et al.* explored a self-assembled fluorescent small-molecule probe (**3**, C-SNAF) for the detection of caspase-3/7 (Fig. 4). The cyclization reaction between free cysteine and CHQ is a biocompatible, kinetically fast intramolecular condensation (6×10^{-3} s^{-1}).[37] After reaction with caspase-3/7 and GSH, the amino and thiol groups of the D-cysteine masked by DEVD and disulfide bonds are released, then, C-SNAF undergoes macrocyclization and *in situ* nanoaggregation, which leads to long residence time and enhanced fluorescence. The caspase-3/7-triggered nano-aggregation of probe **3** enables effective imaging of caspase-3/7 activities *in vivo* and can be used to monitor tumour therapy responses. This is a novel strategy for directing the *in situ* self-assembly of synthetic small molecules into nanoaggregates in living systems.

Recently, Ye *et al.* reported a photoacoustic (PA) probe (**4**, 1-RGD) for caspase-3 detection based on the same self-assembly strategy (Fig. 5).[44] The probe (**4**) consists of a CHQ and a D-cysteine residue, a caspase-3-cleavable peptide substrate DEVD, a glutathione (GSH)-reducible disulfide bond, a tumour tissue-targetable cyclic peptide (c-RGD) and a clinically used near-infrared (NIR) dye (indocyanine green, ICG). Probe **4** can target tumor tissues, since c-RGD targets the $\alpha_v\beta_3$ integrin receptor which is overexpressed in tumor cells. Upon interaction with GSH and caspase-3, free Cys and CHQ underwent fast intramolecular condensation to form a cyclized product, subsequently inducing stronger intermolecular interactions to promote molecular self-assembly into nanoparticles. Thus, probe **4** could realize both PA and fluorescence imaging of caspase-3 activity and distribution within tumour tissues. This work reports the first smart PA probe for real-time monitoring of caspase-3 activity in deep tissues.

Fig. 4 Proposed caspase-3/7 and reduction-controlled conversion of C-SNAF into C-SNAF-cycl through the bioorthogonal intramolecular cyclization reaction, followed by self-assembly into nanoaggregates *in situ*. Reprinted from ref. 37 with permission. Copyright 2014 Macmillan Publishers Limited.

Fig. 3 Illustration of the activity localization fluorescence peptide probe **2** for peptidase imaging. Reprinted from ref. 43 with permission. Copyright 2016 American Chemical Society.
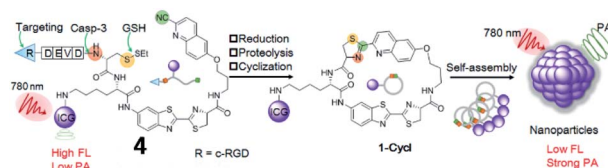

Fig. 5 Development of a PA imaging probe **4** for detecting caspase-3 activity. Reprinted from ref. 44 with permission. Copyright 2019 Wiley-VCH Verlag GmbH & Co. KGaA, Weinheim.
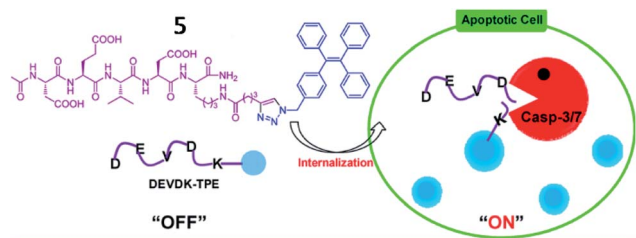
Fig. 6 Illustration of probe **5** for caspase-3/-7 activities. Reprinted from ref. 45 with permission. Copyright 2012 American Chemical Society.

Several AIE-based fluorescent "turn-on" probes for caspase-3 detection have been reported by Tang and co-workers (Fig. 6). In 2012, probe **5** consisting of a DEVD peptide and an AIEgen (TPE, tetraphenylethene) was synthesized to monitor caspase-3/-7 activities from mammalian cells in real time.[45] In the presence of caspase-3/-7, the peptide was cleaved from TPE, resulting in fluorescence recovery of TPE due to the AIE effect. This work provides an effective strategy for real-time imaging of live-cell apoptosis. However, its short emission wavelength limited its application in imaging of apoptosis *in vivo*.

In 2016, another FRET- and AIE-based fluorescent probe (**6**) for caspase-3 detection was developed (Fig. 7).[46] Coumarin chromophore was used as the energy donor and linked with an AIEgen (as an energy acceptor) through the DEVD sequence. Upon encountering caspase-3, the AIEgen was enzymatically released and subsequently aggregated, inducing the recovery of coumarin fluorescence and AIEgen fluorescence. This probe provides "turn-on" of two fluorescence signals during analyte identification, which was used for caspase-3-related drug screening.

Tang *et al.* synthesized a multicolour fluorescent nanoprobe (**7**) for the imaging of caspase-3, -8 and -9 simultaneously during cell apoptosis (Fig. 8a). By attaching caspase peptide substrates labelled with three different fluorophores onto gold nanoparticles through Au–Se bonds, nanoprobe **7** could synchronously visualize the activations of caspase-3, -8, and -9. Utilizing this nanoprobe, the authors revealed that caspase-8 and
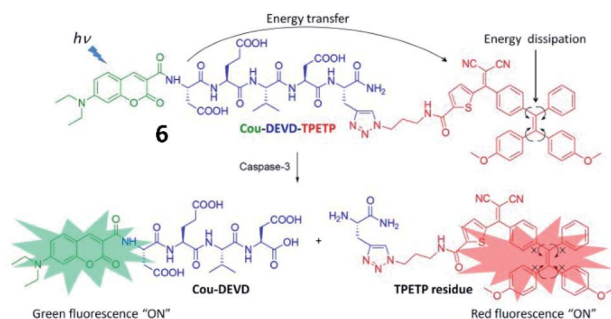

Fig. 7 Schematic illustration of the FRET probe using AIEgen as an energy quencher with dual signal output for self-validated caspase-3 detection. Reprinted from ref. 46 with permission. Copyright 2016 The Royal Society of Chemistry.
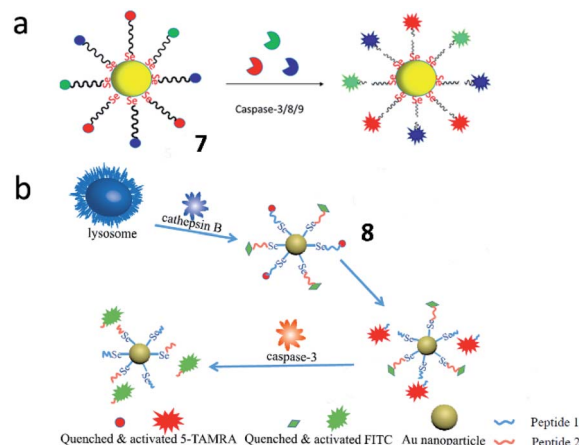

Fig. 8 (a) The structure of probe **7** for monitoring the activities of caspase-3, -8 and -9 simultaneously. Reprinted from ref. 47 with permission. Copyright 2019 American Chemical Society. (b) The structure of probe **8** for monitoring the activities of caspase-3 and cathepsin B. Reprinted from ref. 48 with permission. Copyright 2019 Elsevier Ltd.

caspase-9 could activate caspase-3 during the cell apoptosis process. This nanoprobe is a promising tool for real-time monitoring of caspase cascade activations.[47] Based on this work, the Tang group also developed another Au–Se-bonded nanoprobe (**8**) for fluorescence imaging of caspase-3 and cathepsin B (Fig. 8b). In the presence of caspase-3 and cathepsin B, the peptide chains with fluorophores were specifically cleaved by caspase-3 or cathepsin B, leading to fluorescence recovery. This work confirmed that cathepsin B and caspase-3 were sequentially activated in cancer cells during apoptosis. Both probes **7** and **8** could be effective tools for understanding the cell apoptotic mechanisms.[48]

3.1.2 Fluorescent probes for aminopeptidase N. Aminopeptidase N (APN) is a Zn^{2+}-dependent metalloprotease belonging to the M1 family, which is present in a wide variety of human tissues and cell types. It consists of 967 amino acids and is located on the cell membrane as a type-II integral membrane protein.[49] APN is an essential peptidase involved in the process of tumour angiogenesis, metastasis, cell differentiation, proliferation and apoptosis.[50,51] In tumour cells, APN is overexpressed on the endothelial cell surface as a receptor of NGR (a tumour-homing peptide motif, Asn–Gly–Arg). Moreover, an inhibitor of APN, ubenimex, was reported to induce apoptotic cell death in rat pituitary tumour cells by promoting ROS generation.[52] Therefore, several fluorescent probes for imaging of tumour tissues and drug screening through the targeting of APN have been created.[53,54]

Li *et al.*[55] reported three ratiometric fluorescent probes **9–11** for detecting the activities of APN (Fig. 9). They chose 1,8-naphthalimide, a prototype ICT fluorophore as a reporter, and alanine and norvaline as the recognition moieties. After the cleavage of the amide bond between the amino acids and the fluorophores by APN, 1,8-naphthalimide can be released and the ICT effect is enhanced.
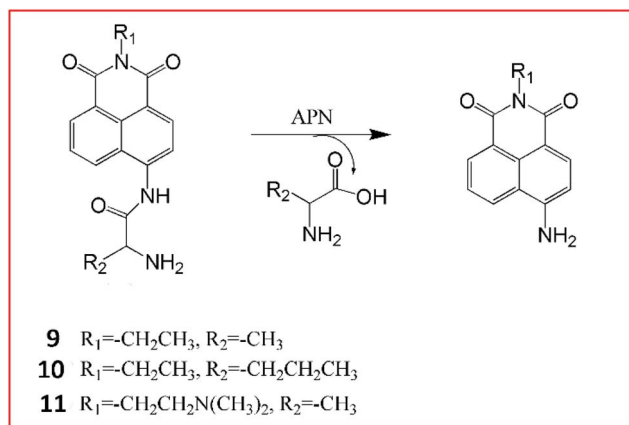
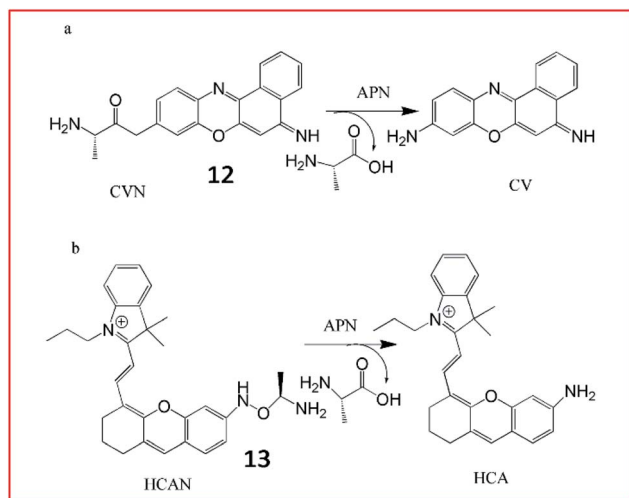**Fig. 9** Detection mechanism of probes **9–11** for detecting the activities of APN.

Fig. 10 Structure of probes **12** and **13** and detection mechanism with APN.

Fig. 11 Structure of probes **14** and **15** and their detection mechanism with APN.

The maximum fluorescence emission redshifts from blue fluorescence to a strong bright green fluorescence.[55]

Ma *et al.* developed an ultrasensitive ratiometric fluorescent probe (**12**, CVN) to visualize APN (Fig. 10a).[56] The amino substitution by alanine caused a distinct blue-shift of the fluorescence peak from 626 to 575 nm. After reaction with APN, the fluorescence intensity of the probe at 575 nm decreased and that at 626 nm increased gradually. The detection limit of CVN was determined to be 33 pg mL^{-1}, suggesting that **12** was an ultrasensitive probe for detecting APN, making it the most sensitive APN-detecting fluorescent probe known. The same group further explored another NIR fluorescent probe (**13**, HCAN) for detection of APN in 2017 (Fig. 10b).[57] The NIR dye hemicyanine was used as the fluorescence-reporting moiety and an alanine residue was taken as the recognition group. The amino substitution by alanine efficiently quenches the fluorescence of hemicyanine, since the electron-withdrawing effect of the amide bond disturbs the conjugation of the fluorophore.
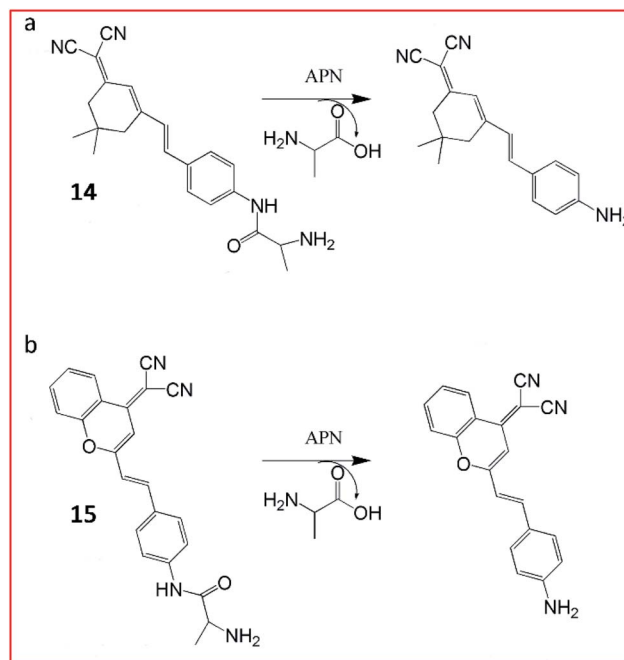
After reaction with APN, the amide bond is cleaved to release the fluorophore and emit strong fluorescence. Probe **13** was the first NIR-based fluorescent probe for imaging of APN with high selectivity and sensitivity.

For tracking metastatic cancer and imaging tumours during surgery, Peng and Yoon *et al.* developed an APN-activatable fluorescent probe (**14**, YH-APN; Fig. 11a).[58] The probe was constructed with a dicyanoisophorone as the fluorescence-reporting group and L-alanine as the recognition group for APN, which emitted strong NIR fluorescence upon APN cleavage. The probe (**14**) was able to monitor the activity of APN in cancer cells with ultrasensitivity and excellent selectivity. This probe could also be successfully lighted up in tumour cells, exhibiting great potential for image-guided surgery.

Peng *et al.* reported a two-photon NIR fluorescence probe (**15**, DCM-APN) to track APN *in vivo* (Fig. 11b).[59] The probe contained an L-alanine as the substrate of APN and a dicyanomethylene-benzopyran (DCM) as the chromophore. Probe **15** had been successfully employed to distinguish normal cells (LO2 cells) from cancer cells (HepG-2 and B16/BL6). Furthermore, the probe could be used to investigate the activity of APN in hepatocellular carcinoma tissues *in situ*. The NIR excitation and emission wavelengths provided the deep-tissue imaging opportunity for the probe.

3.1.3 Fluorescent probes for matrix metalloproteinases. Matrix metalloproteinases (MMPs) are a family of endogenous proteases, consisting of 23 members (including MMP-3, MMP-7 and so on), which play a pivotal role in maintaining and reconstructing extracellular matrix by degrading extracellular matrix proteins.[60] MMPs participate in several physiological and pathological processes, such as wound healing, inflammation,
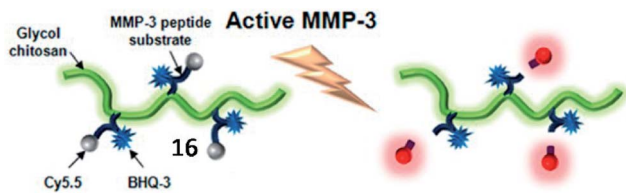
Fig. 12 Schematic diagram of the MMP-3 probe **16**. When MMP-3 encounters the specific substrate recognition site of the probe, a pronounced NIR fluorescence signal recovery is observed. Reprinted from ref. 68 with permission. Copyright 2013 American Chemical Society.

Fig. 14 Chemical structure of MMP probe **18**. Reprinted from ref. 70 with permission. Copyright 2015 American Chemical Society.

arthritis, cardiovascular disease and cancer.[61] Previous studies have shown that the activities of MMPs are often associated with ROS levels in cancer cells. For example, tetrabromobisphenol A can activate MMP-9 by ROS-dependent mitogen-activated protein kinase pathways to induce human breast carcinoma MCF-7 cell metastasis.[62] Correspondingly, the decrease in ROS can reduce the activities of MMP-2 and MMP-9, thereby attenuating cell motility of human fibrosarcoma cells.[57,63]

Consequently, several ROS-associated MMPs are considered potential diagnostic and prognostic biomarkers for cancers.[64–66]

Until now, a large number of MMP-responsive fluorescent probes for imaging have been successfully developed, all of which were designed by incorporating chromophore-modified substrates and a quencher.[67] Youn et al. developed a soluble probe, **16**, for detecting the activity of MMP-3 from serum to monitor the progress of rheumatoid arthritis (Fig. 12).[68] This MMP-3 probe was constructed with a peptide (GVPLSLTMGK) modified with a dark quencher 3 (BHQ-3) and an NIR fluorophore (Cy5.5) and glycol chitosan (GC). After being specifically cleaved by MMP-3, Cy5.5 was released and the NIR fluorescence signal in the probe was restored. This MMP-3 probe was used to selectively detect the activity of MMP-3 in diluted serum from CIA mice.
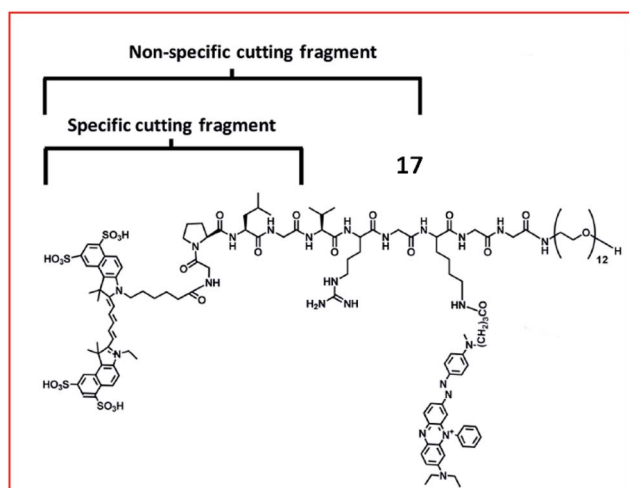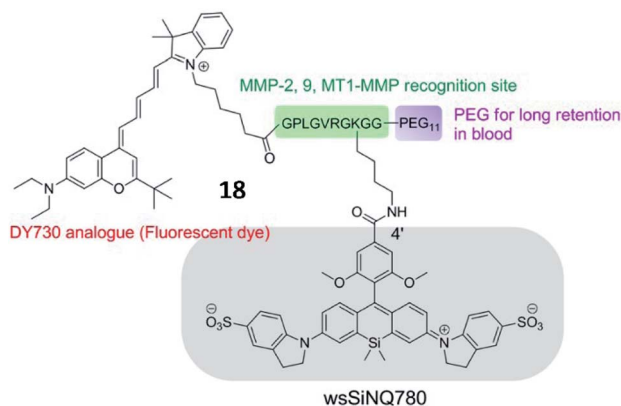
Chen et al. developed an MMP-13 probe (**17**, D-MMP-P12) to image MMP-13 activity in vivo. D-MMP-P12 contained a Cy5.5 dye, an MMP substrate (GPLGVRGKGG), a quencher BHQ-3, and a polyethylene glycol (PEG)-12 chain (Fig. 13).[69] Specific cleavage of the peptidase substrate in D-MMP-P12 by MMP-13 generated strong fluorescence enhancement of Cy5.5. This probe could be used to visualize MMP-13 activity in squamous cell carcinoma (SCC)-7 tumour-bearing mice. A similar strategy was employed by Urano and coworkers, who designed a FRET-based NIR fluorescent probe **18** for the determination of MMP activities (Fig. 14).[70] Upon being cleaved by MMPs, the fluorescent dye was cleaved off the probe, departed from the quencher and emitted NIR fluorescence. This probe could detect MMP activity in vitro, in cultured cells and in tumour-bearing mice.

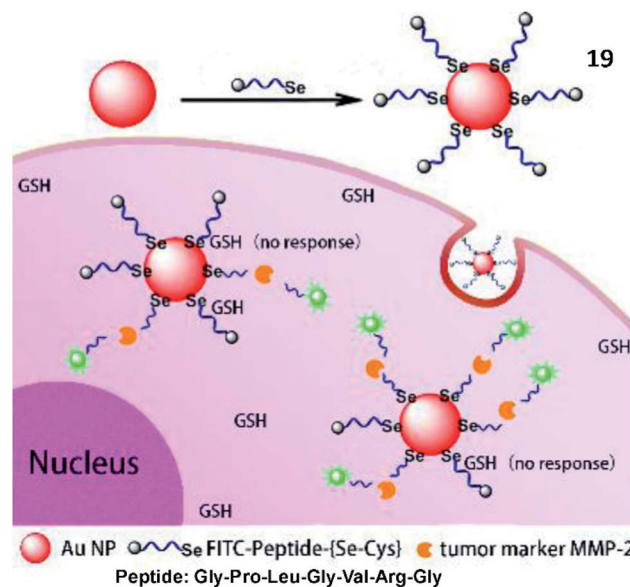Tang et al. developed an Au–Se bond based nanoprobe for detection of MMP activities with anti-interference ability for

Fig. 13 Structure of MMP probe **17**. Reprinted from ref. 69 with permission. Copyright 2013 American Chemical Society.

Fig. 15 Structure of probe **19** and detection mechanism with MMP-2. Reprinted from ref. 71 with permission. Copyright 2018 American Chemical Society.

glutathione (Fig. 15).[71] Although the Au–Se bond and Au–S bond possessed similar physical and chemical properties, the Au–Se bond showed higher stability than the Au–S bond. The probe (**19**) was an easily assembled nanosensor, which was coupled with a selenol- and FITC-modified Gly–Pro–Leu–Gly–Val–Arg– Gly (the specific substrate of MMP-2) peptide onto the surface of AuNPs. Compared to the commonly used Au–S probes, the Au– Se probes display high thermal stability and good anti-interference ability towards glutathione.

In addition, Zhang *et al.* developed a multi-FRET fluorescent probe (**20**, Mc-probe) for simultaneous imaging of MMP-2 and caspase-3 activities (Fig. 16).[72] Mc-probe was constructed with an MMP-2 sensitive peptide (GPLGVRG), a caspase-3 specifically responsive peptide (SDEVDS), and fluorophores (5(6)-carboxy-fluorescein (FAM)/tetramethylrhodamine (TAMRA)/Dabcyl). The fluorescence of FAM and TAMRA was initially quenched due to the FRET process. After being cleaved by MMP-2, FRET between TAMRA and Dabcyl was blocked, restoring TAMRA fluorescence. After further cleavage by caspase-3, FAM fluorescence was recovered due to the blockade of FRET between FAM and TAMRA. These kinds of fluorescent probes designed for simultaneous imaging of different enzymes have great potential for precise disease diagnosis and therapeutic efficacy evaluation.

Moreover, an MMP-2-responsive PA and fluorescent probe (**21**, QC) was developed by Gao and coworkers (Fig. 17).[73] The probe was established by the covalent linkage of an NIR dye
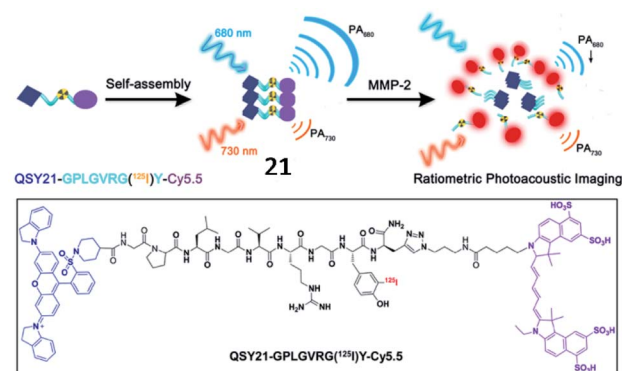

Fig. 17 Probe **21** for non-invasive detection of MMP-2 activity through fluorescence and photoacoustic imaging. Reprinted from ref. 73 with permission. Copyright 2019 American Chemical Society.

(Cy5.5) and a quencher (QSY21) with the MMP-2 cleavable peptide (GPLGVRGY). Probe **21** self-assembled into nanoparticles in aqueous solution due to the presence of both a hydrophilic group (Cy5.5) and hydrophobic group (QSY21). When probe **21** was cleaved by MMP-2, the fluorophore Cy5.5 was released, emitting NIR fluorescence and a PA signal. Utilizing NIR/PA dual imaging, the fluorescence probe **21** could quantitatively detect MMP-2 with deep-penetration in tumour tissues from 4T1 tumour-bearing nude mice.

Xia *et al.* developed an MMP-2 activatable probe (**22**, DOX-FCPPs-PyTPE, DFP) to image MMP-2 activity and deliver drugs *in vivo* (Fig. 18).[74] Probe **22** contained a TPE derivative (PyTPE) as the AIE-active unit, a functionalized cell penetrating peptide (FCPPs, CRRRRRRRRRP), a short MMP-2 specific substrate (LGLAG), and a therapeutic unit (doxorubicin, DOX). After being cleaved by MMP-2, the released hydrophobic PyTPE aggregated, generating strong yellow fluorescence. Then, the hydrophilic FCPPs-DOX could quickly permeate into MMP-2 overexpressed cells. This probe could distinguish different cell types which possessed varied MMP-2 activities, and also has high cytotoxicity to MMP-2 over-expressed cells. This work could be a milestone in MMP-2 related theranostics.
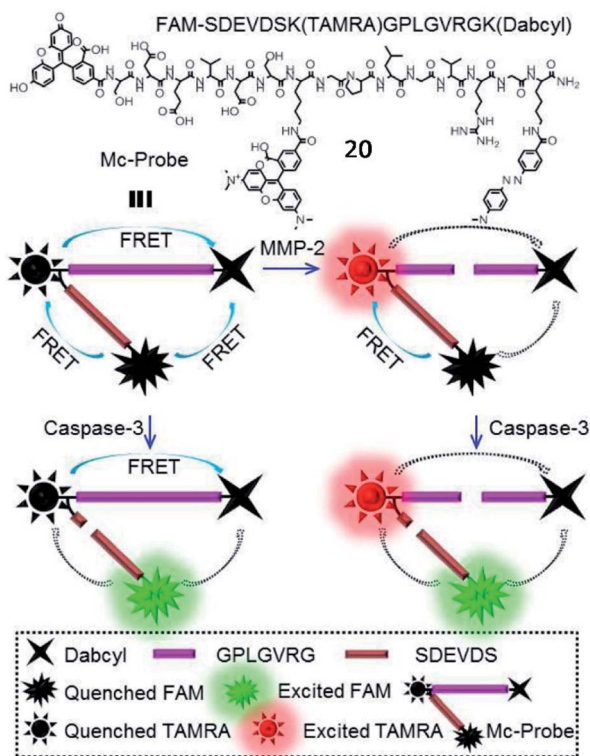

Fig. 16 Chemical structure and the proposed processes of probe **20** for spatiotemporal MMP-2 and caspase-3 imaging. Reprinted from ref. 72 with permission. Copyright 2017 American Chemical Society.
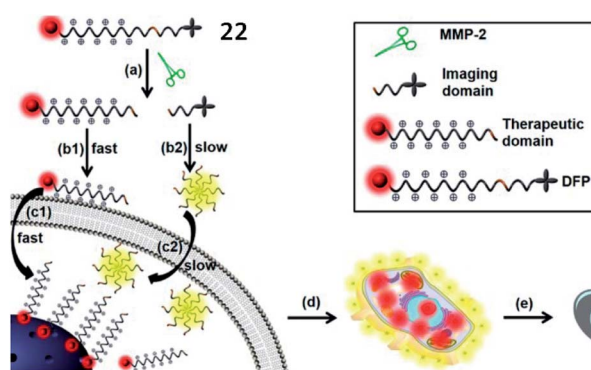

Fig. 18 Probe **22** for rapid drug delivery and release tracking in MMP-2 over-expression living cells. Reprinted from ref. 74 with permission. Copyright 2016 American Chemical Society.

3.1.4 Fluorescent probes for cathepsin. Cathepsins are a family of lysosomal cysteine proteases, which include more than a dozen cathepsins. In cancer cells, cathepsin B and cathepsin L are associated with the plasma membrane to hydrolyse the extracellular matrix, playing essential roles in tumour invasion and metastasis. In addition, many reports have shown that the ROS level in cells could be mediated by cathepsin activities. Inhibition of cathepsin B significantly reduces the generation of ROS in microglia.[75] Moreover, cathepsin S can regulate the PI3K/Akt (phosphoinositide 3-kinases/protein kinase B) signalling by mediating ROS in human glioblastoma cells.[76] To date, several fluorescent probes have been developed for imaging the activities of cathepsin B and L *in vivo* and differentiation between cancer and normal tissues.[77,78]

Several cathepsin activatable small-molecule probes have been created for fluorescence imaging *in vivo*. Chen *et al.* developed a lysosome-targeting probe (**23**) to sense cathepsin B activity in living cancer cells (Fig. 19).[79] The probe was incorporated by a cathepsin B-recognitive peptide substrate Cbz–Lys–Lys–*p*-aminobenzyl alcohol (Cbz–Lys–Lys–PABA) and a lysosome locating group morpholine. The fluorescence intensity of the probe increased 73-fold upon cathepsin B-mediated cleavage of the substrate, suggesting that the probe possessed high sensitivity toward cathepsin B.

Kim *et al.* explored a fluorescent probe (**24**, RR-S-Ac3Man-NAz) for the detection of cathepsin B activity by incorporating a cathepsin B-specific substrate (Lys–Gly–Arg–Arg, KGRR) into a tri-acetylated *N*-azidoacetyl-D-mannosamine (Fig. 20).[80] After being cleaved by cathepsin B in cells, the released S-Ac3ManNAz could be hydrolysed to produce Ac3ManNAz, which was eventually labelled by a dibenzylcyclooctyne-modified NIR dye (Cy5.5) through bioorthogonal click chemistry. This strategy showed promise for the inspection of enzyme activities *in vitro* and *in vivo*.
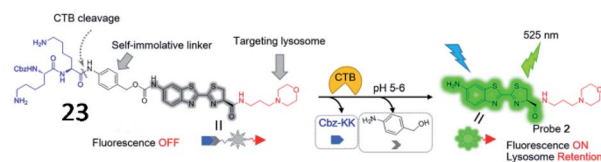

Fig. 21 Illustration of near-infrared imaging and phototherapy of cathepsin B using the probe **25**. Reprinted from ref. 81 with permission. Copyright 2017 Elsevier Ltd.

In addition, several fluorescent probes for simultaneous imaging and treatment of cancer have been reported. Yoon *et al.* described a cathepsin B-activated fluorescent probe (**25**, CyA-P-CyB) for detecting cathepsin B activity and investigated its application in imaging tumour tissues *in vivo* (Fig. 21).[81] The probe (**25**) consisted of two cyanine moieties (CyA and CyB), linked by a cathepsin B-activated peptide (Gly–Phe–Leu–Gly). After being cleaved by cathepsin B, the probe released two chromophores, evoking two fluorescence signals. This probe also exhibited great phototoxicity to tumour cells in mice, thus providing great potential for tumour treatment.

Liu and Tang *et al.* described a cathepsin B-activatable probe (**26**) based on an AIEgen, which could simultaneously image and treat cancer though photodynamic therapy (Fig. 22).[82] The probe is composed of four parts: (1) an AIE fluorogen as an imaging reagent and photosensitizer, (2) a peptide substrate of cathepsin B, (3) a hydrophilic linker, and (4) a cRGD-targeting moiety. After cancer-cellular uptake, the fluorescence of the probe (**26**) was dramatically enhanced due to the AIE effect upon

Fig. 19 The chemical structure of probe **23** and the proposed chemical conversion in response to cathepsin B. Reprinted from ref. 79 with permission. Copyright 2016 American Chemical Society.
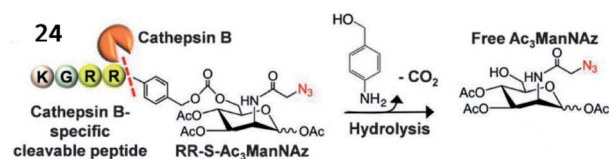

Fig. 20 Probe **24** for rapid drug delivery and release tracking in MMP-2 over-expression living cells. Reprinted from ref. 80 with permission. Copyright 2016 American Chemical Society.
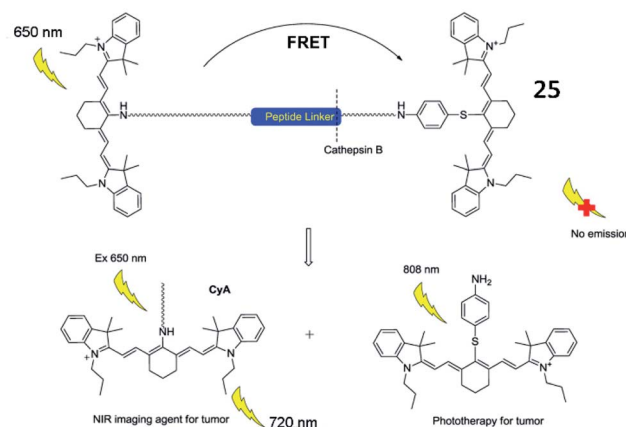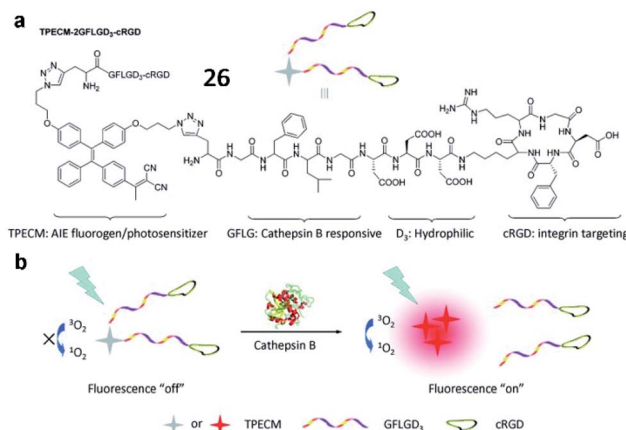

Fig. 22 The chemical structure of probe **26** and the proposed chemical conversion in response to cathepsin B. Reprinted from ref. 82 with permission. Copyright 2016 American Chemical Society.

cleavage of the GFLG peptide by cathepsin B, and the PDT was activated. Probe **26** could be used for image-guided PDT in cancer cells. These studies provide valuable strategies for the development of probes for cancer diagnosis and treatments.

3.1.5 Fluorescent probes for tyrosinase. Tyrosinase (TYR, EC 1.14.18.1), a copper-containing monooxygenase that catalyses the hydroxylation and oxidation of phenol derivatives (such as tyrosine or tyramine) to the corresponding *o*-quinone products, is widespread in plants, animals, and microorganisms.[83] Molecular oxygen is necessary for enzymatic reactions in living systems.[84] Studies have indicated that tyrosinase can eliminate ROS in the skin by utilizing superoxide to produce melanin.[85] In addition, tyrosinase activity can be induced by intracellular H_2O_2, suggesting a strong association between tyrosinase and ROS.[86] In humans, abnormal tyrosinase activity is responsible for severe skin diseases, dopamine neurotoxicity, and neuro-degeneration. Notably, tyrosinase is a significant biomarker of melanoma cancer due to its overexpression in melanoma cells.[87,88] Therefore, the sensitive and selective assessments of this biochemical marker by fluorescence imaging would be highly valuable for investigating its biological roles and value in disease diagnosis.

Many tyrosinase activity-based fluorescent probes with a tyrosinase substrate and fluorophore have been constructed to image tyrosinase activity *in vivo*. Ma *et al.* synthesized a small-molecule "off–on" fluorescent probe (**27**, Mela-TYR) to monitor tyrosinase in cells (Fig. 23a). This probe was engineered by engineering 4-aminophenol-derived urea and morpholine into a naphthalimide scaffold, and morpholine was used as a mela-nosome-targeting group. Upon the enzymatic cleavage of **27**, the naphthalimide fluorescence recovered. This probe provides a practical tool to investigate the activity of tyrosinase in cells.[89]

Subsequently, several fluorescent probes were developed following the above strategy. Zhang *et al.* developed a resorufin-based fluorescent probe (**28**) for the detection of tyrosinase (Fig. 23b). *m*-Tolylboronic acid pinacol ester was used as a substrate for tyrosinase; thus, resorufin was released in the
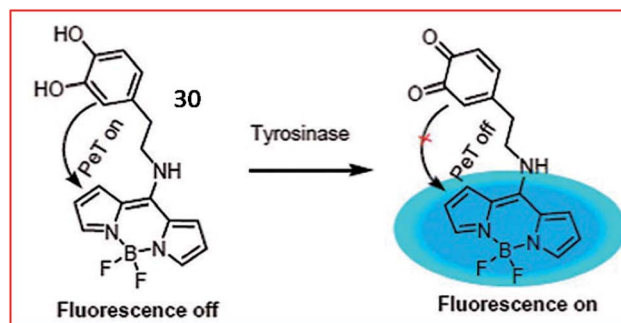

Fig. 24 Fluorescence changing mechanism of probe **30** in the presence of tyrosinase. Reprinted from ref. 86 with permission. Copyright 2017 The Royal Society of Chemistry.

presence of tyrosinase. This probe exhibits high selectivity and sensitivity towards tyrosinase, suggesting its use as a promising tool for the detection of tyrosinase in biosystems.[90]

Wu *et al.* developed a fluorescent probe (**29**, NBR-AP) to sense tyrosinase by modifying a phenoxazine derivative with a hydroxyphenyl urea group (substrate for tyrosinase) (Fig. 23c). In the presence of tyrosinase, the carbamide bond broke, and the fluorescent dye was released, emitting strong fluorescence. Probe **29** could selectively detect tyrosinase activity in cells and living zebrafish. Moreover, based on changes in tyrosinase activity, the probe could indicate melanoma metastasis in a mouse model.[91]

A PeT-based two-photon fluorescent probe (**30**, Tyro-1) was designed by Bhuniya and coworkers to track the activity of intracellular tyrosinase (Fig. 24). BODIPY was chosen as the chromophore due to its photophysical stability, large Stokes shift and high quantum yield. The tyrosinase activity in various cell types was detected by probe **30**. Moreover, utilizing the probe, the authors disclosed that H_2O_2 can promote tyrosinase activity in cells.[86]

Since previously reported fluorescent probes for tyrosinase showed similar responses to both tyrosinase and some reactive oxygen species (ROS), thereby suffering from the ROS interferences, Ma *et al.* proposed a new tyrosinase-recognition moiety, 3-hydroxybenzyloxy, in which the presence of the unique 3-hydroxy (instead of 4-hydroxy) group facilitates the hydroxyl-ation at the 4-position vacancy by tyrosinase but not by ROS, and the resulting hydroxylation unit would be spontaneously removed by the subsequent 1,6-rearrangement–elimination (Fig. 25a).[92] The probe (**31**) can specifically identify tyrosinase instead of ROS. The probe consisted of a 3-hydroxybenzyloxy moiety as a new recognition unit and a stable hemicyanine group as a fluorescent reporter, which can be used to detect endogenous tyrosinase activity in live cells and zebrafish.

Recently, Ding *et al.* reported a hydrosoluble NIR fluorescent probe (**32**) to image tyrosinase activity by using 3-hydrox-ybenzyloxy as the substrate of tyrosinase too (Fig. 25b). In the presence of tyrosinase, the maximum absorption wavelength of the probe was red-shifted from 600 nm to 670 nm, and the fluorescence intensity at 708 nm was significantly enhanced.
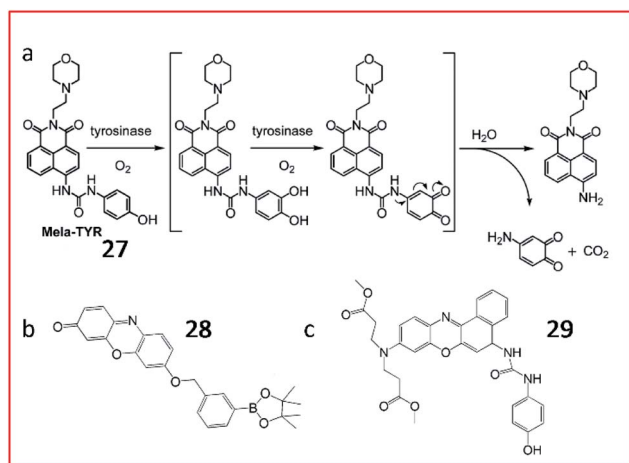

Fig. 23 (a) Probe **27** reaction with tyrosinase. Reprinted from ref. 89 with permission. Copyright 2016 American Chemical Society. (b) Structure of probe **28**. (c) Structure of probe **29**.
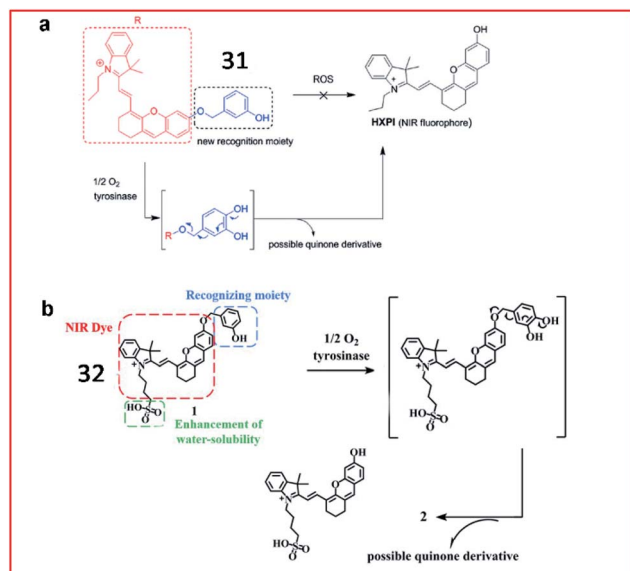
Fig. 25 (a) The proposed reaction mechanisms of probe **31** with tyrosinase and ROS. Reprinted from ref. 92 with permission. Copyright 2016 Wiley-VCH. (b) Probe **32** reaction with tyrosinase. Reprinted from ref. 93 with permission. Copyright 2019 The Royal Society of Chemistry.

Fig. 26 Proposed mechanism of probe **33** with γ-GGT. Reprinted from ref. 108 with permission. Copyright 2016 The Royal Society of Chemistry.

This probe (**32**) was successfully used to monitor tyrosinase activity in cells and mice.[93]

Many other fluorescent probes have also been developed for the fluorescence imaging of tyrosinase activity.[94–97] Su *et al.* designed a ratiometric fluorescence probe, containing red-emissive QDs and green-emissive QDs as fluorophores to provide ratiometric signals. Dopamine and QDs were conjugated to the surface of silica nanoparticles. Upon reaction with tyrosinase, dopamine transformed into dopamine quinine, thereby quenching the fluorescence of the green QDs. By monitoring the green and red fluorescence intensities, tyrosinase activity could be quantified.[98] In 2018, Ouyang *et al.* reported a PeT-based NIR fluorescent probe (HB-NP) with a large Stokes shift (195 nm) for the detection of tyrosinase.[99] HB-NP showed high selectivity towards tyrosinase and successfully realized the quantitative detection of tyrosinase in diverse living cells, especially in melanoma cells. In 2011, a BODIPY-based "turn-on" fluorescent probe to assess the activity of tyrosinase and the effect of tyrosinase inhibitors was presented by the Kim group.[100]

3.1.6 Fluorescent probes for γ-glutamyltranspeptidase. γ-Glutamyltranspeptidase (γ-GGT) is a cell membrane binding protease essential for maintaining cysteine homeostasis and regulating intracellular redox status. GGT participates in the upregulation of oxidative stress by cleaving GSH and other γ-glutamyl compounds to balance the redox state in cells.[101,102] Abnormal GGT activity is associated with many diseases, such as liver dysfunction, asthma, reperfusion injury, diabetes, and cancer.[103–105] Furthermore, elevated GGT activity in the serum is a common diagnostic marker of several diseases, such as liver, ovar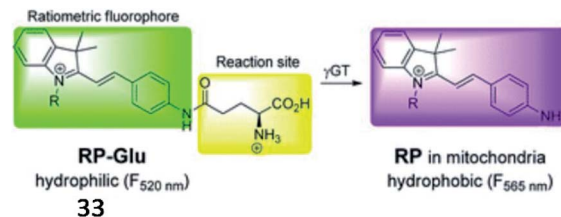ian and pancreatic cancers.[106,107] Therefore, fluorescence imaging and quantification of GGT activity could contribute to cancer diagnosis.

Over the past decade, several fluorescent probes have been reported to detect the activity of GGT. Kim *et al.* reported a mitochondria-targeted ratiometric probe (**33**, RP-Glu); the acid moiety of AP-Glu was replaced with an ester group, and an amide group was directly conjugated to indocyanine (Fig. 26). Probe **33** initially showed weak luminescence in a shorter wavelength region because of its amide functionality. When exposed to γ-GGT, the probe displayed strong fluorescence at the far-green region of the spectra through the enzyme-mediated amide bond cleavage reaction. This probe presented a ratiometric fluorescence response in cellular mitochondria and could detect cancer in mouse colons by imaging mitochondrial GGT activity.[108]

Li and Xu *et al.* reported a ratiometric GGT-responsive sensor (**34**, Py-GSH) with high sensitivity. The probe consisted of a GSH group as the GGT-responsive moiety and pyronin B as the fluorescent group (Fig. 27). After reaction with GGT, the GSH group was cleaved, and electron rearrangement of Py-CG occurred, yielding strong green fluorescence at 540 nm. Probe **34** could rapidly and selectively track GGT activity in GGT-positive small peritoneal metastatic tumours (∼1 mm in diameter) in a mouse model. Moreover, this probe could detect microscopic cancer nodules in clinical tumour resection.[109]

In addition, several NIR fluorescent probes were also developed for the detection of γ-GGT. Li *et al.* synthesized a zero cross-talk ratiometric NIR fluorescent probe (**35**, Cy-GSH) consisting of cyanine as a chromophore and GSH as the GGT-recognition unit to sense the activity of GGT (Fig. 28).[110] Upon reaction with GGT, the γ-glutamyl moiety of probe **35** was removed, and the maximum emission wavelength was blue-shifted from 805 nm to 640 nm. Probe **35** could detect GGT in the blood, cells, and tumour tissues with high sensitivity and

Fig. 27 The presence of GGT leads to γ-glutamyl cleavage of **34**. Reprinted from ref. 109 with permission. Copyright 2021 Ivyspring International Publisher.
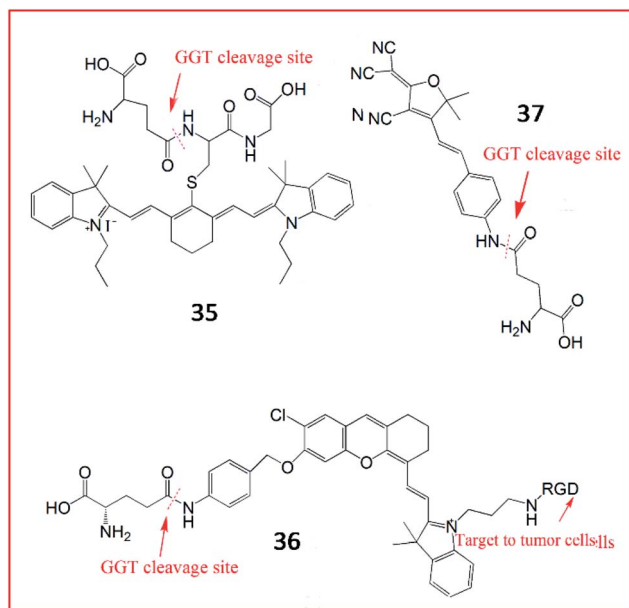
Fig. 28 The structures of probes **35–37**. These probes were used to detect the activity of GGT.

a low detection limit. Chen *et al.* also developed an NIR fluorescence sensor (**36**) constructed with hemicyanine dye as a signalling moiety, *p*-aminobenzyl alcohol as a self-immolative linker, γ-Glu as a substrate and c-RGD as the tumour-targeting group.[111] Upon GGT catalysis against the self-immolative linker of probe **36**, the free NIR dye was released, producing a strong fluorescence signal. This probe successfully targeted tumour cells in living mice in a non-invasive manner by $\alpha_v\beta_3$ receptor-mediated endocytosis. In the same year, another light-up NIR fluorescent probe (**37**, DCDHF-Glu) was developed by the Kong group.[112] The probe **37** contained a dicyanomethylene dihydrofuran derivative as the signal reporter unit and a γ-glutamyl group as the enzyme-active trigger moiety. In the presence of GGT, the recognized substrate of GGT was removed, accompanied by a "turn-on" fluorescence response based on ICT.

In addition, many other fluorescent probes have been developed over the past decade to sense the activity of GGT.[113–116] For instance, Wang *et al.* reported the fluorescent probe NM-GSH, which was composed of a γ-glutamyl group as a substrate of GGT and 1,8-naphthalimide as a chromophore. This probe could selectively image ovarian cancer cells.[117] Peng *et al.* explored a two-photon fluorescent probe, TCF-GGT, by modifying a γ-GGT enzyme-specific substrate to 2-dicyanomethylene-3-cyano-4,5,5-trimethyl-2,5-dihydrofuran derivatives.[118] Specific cleavage of the amide bond in the probe by γ-GGT released an electron-donating amine moiety to generate TCF-NH$_2$, inducing remarkable fluorescence enhancement. This probe was applied for the identification of ovarian cancer cells from normal cells and real-time tracking of γ-GGT activity in a tumour xenotransplantation model in mice. Moreover, Urano *et al.* synthesized several fluorescent probes for the detection of GGT. The highly sensitive fluorescence probe gGlu-HMRG and the rhodamine-based fluorescent probe gGlu-

HMJCR were manufactured to detect lysosomal GGT activities in ovarian cancer. Furthermore, the authors designed the fluorescent probe gGlu-HMJSiR for real-time monitoring of GGT activity in cells.[119–121]

3.1.7 Fluorescent probes for β-galactosidase. β-Galactosidase (EC 3.2.1.23) is a lysosomal hydrolase that plays a vital physiological role in hydrolysing D-galactosyl residues from polymers, oligosaccharides and secondary metabolites. This enzyme is widely used in the food industry to remove lactose from milk products to produce galactosylated food for lactose-intolerant people.[122,123] β-Galactosidase can be found in many groups of species, including microorganisms, plants and animals. Abnormal β-galactosidase activity in humans is associated with cell senescence, AD and type 2 diabetes. Moreover, overexpression of β-galactosidase is often correlated with the occurrence of primary ovarian cancers, as β-galactosidase can disintegrate macromolecular proteoglycan and destroy the extracellular interstitial barrier.[124] Hence, fluorescent probes developed for the accurate and effective detection of β-galactosidase can monitor its fundamental activity and track the metastasis of cancer cells.

In 2011, Urano and Nagano *et al.* created a fluorescent probe (**38**, HMDER-βGal) in which a β-galactopyranoside group was incorporated into the hydroxymethyl group (HMDER) of the scaffold for the detection of β-galactosidase activity (Fig. 29a).[125] The fluorescence intensity of probe **38** obviously increased upon reaction with β-galactosidase. This is the first fluorescent probe in which spirocyclization of a hydroxymethyl group was utilized to control fluorescence emission upon reaction with the enzyme at physiological pH. In 2015, the authors developed a new fluorescent probe (**39**, HMRef-βGal) that exhibited bright fluorescence (>1400-fold fluorescence enhancement) upon the addition of β-galactosidase due to its optimized intramolecular spirocyclic effect (Fig. 29b).[126] Probe **39** was successfully applied to diagnose cancer and mark tumour metastases *in vivo* with high sensitivity.

Several activatable ratiometric fluorescent probes have been designed to quantitate β-galactosidase activity. Lin *et al.*
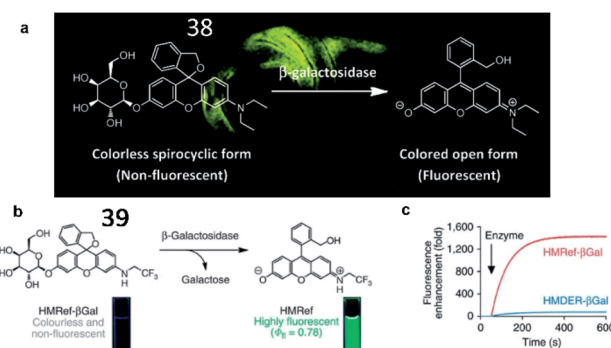

Fig. 29 (a) The proposed reaction mechanisms of probe **38** with β-galactosidase. Reprinted from ref. 125 with permission. Copyright 2011 American Chemical Society. (b) Activation of **39** on enzymatic reaction with β-galactosidase. (c) Time course of the enzymatic reaction of **39** with β-galactosidase. (b) and (c) Reprinted from ref. 126 with permission. Copyright 2015 Macmillan Publishers Limited.
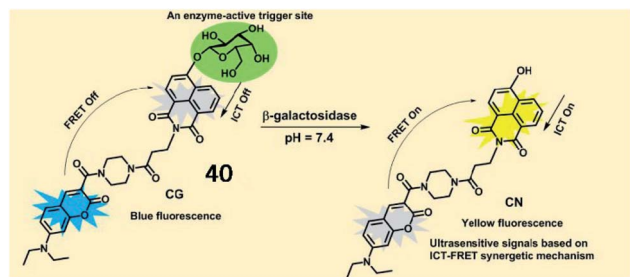
Fig. 30 The proposed reaction mechanisms of probe **40** with β-galactosidase. Reprinted from ref. 127 with permission. Copyright 2019 American Chemical Society.

designed an ICT-FRET-based ratiometric fluorescent probe (**40**, CG) to detect β-galactosidase activity (Fig. 30). In probe **40**, 7-diethylamino coumarin was incorporated as a fluorescent donor, and 4-hydroxy-1,8-naphthalimide was incorporated as an acceptor in a FRET pair. In the presence of β-galactosidase, the specific substrate β-D-galactopyranoside was hydrolysed and released from the probe, which was accompanied by the restoration of fluorescence based on the ICT effect. Probe **40** exhibited a fast response rate (less than 20 s) and a low detection limit (0.081 U mL^{-1}) for β-galactosidase. This probe displays great potential for revealing the function of β-galactosidase in biological organisms.[127]

To achieve deeper tissue penetration, a ratiometric NIR fluorescent probe (**41**, DCM-βgal) to quantify the activity of β-galactosidase was reported by Zhu and coworkers (Fig. 31).[128] The chromophore dicyanomethylene-4H-pyran was utilized as a fluorescent reporter, and a cleavable β-galactosidase moiety was used as an enzyme-active trigger. The emission peak at 685
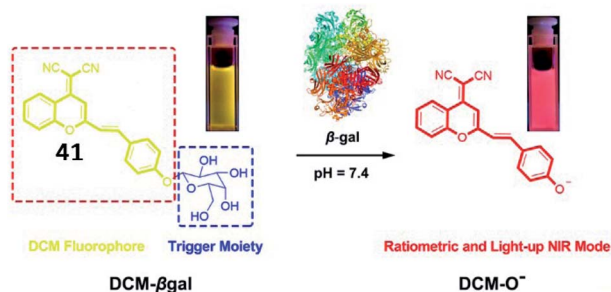
nm was enhanced upon incubation with β-galactosidase. The probe could be used for the ratiometric tracking of endogenously overexpressed β-galactosidase distribution in living 293T cells. This work provides a potential tool for *in vivo* real-time tracking of enzyme activity in preclinical applications.

Kim *et al.* developed another ratiometric NIR fluorescent probe (**42**, DCDHF-βgal) for non-invasive imaging of β-galactosidase (Fig. 32).[129] The maximum emission band was red-shifted from 615 nm to 665 nm upon the activation of probe **42** by β-galactosidase, indicating that the activity of β-galactosidase could be ratiometrically monitored by this probe. Furthermore, probe **42** could detect hepatocellular carcinoma with high selectivity and sensitivity by sensing β-galactosidase overexpression.

Subsequently, several fluorescent probes were developed based on the same strategy shown in Fig. 32. Liu *et al.* reported a lysosome-targeting NIR fluorescent probe (**43**, Lyso-Gal) for the visualization of lysosomal β-galactosidase *in vivo* (Fig. 33). Probe **43** consisted of hemicyanine as the fluorophore and galactose as the recognition group. Upon reaction with β-galactosidase, Lyso-OH, which emitted bright fluorescence, was produced. With its beneficial high sensitivity and ultra-fast response (~1 min) to β-galactosidase, probe **43** could successfully visualize endogenous β-galactosidase in ovarian cancer cells.[130] Compared with other reported probes, probe **43** showed the fastest response to β-galactosidase to date.

As reported in a recent study, Gu *et al.* developed an NIR-II fluorescent probe (**44**, BOD-M-β-gal) for the detection of β-galactosidase (Fig. 33). Probe **44** showed bright fluorescence after cleavage by β-galactosidase. Overexpression of β-galactosidase was visualized by probe **44** with NIR-II emission at 900–1300 nm. Probe **44** could be applied to detect and bio-image

Fig. 31 Proposed sensing mechanism for β-galactosidase enzymatic activation of **41**. Reprinted from ref. 128 with permission. Copyright 2016 American Chemical Society.

Fig. 32 Conceptual scheme of **42** when encountering β-galactosidase. Reprinted from ref. 129 with permission. Copyright 2017 Elsevier Ltd.

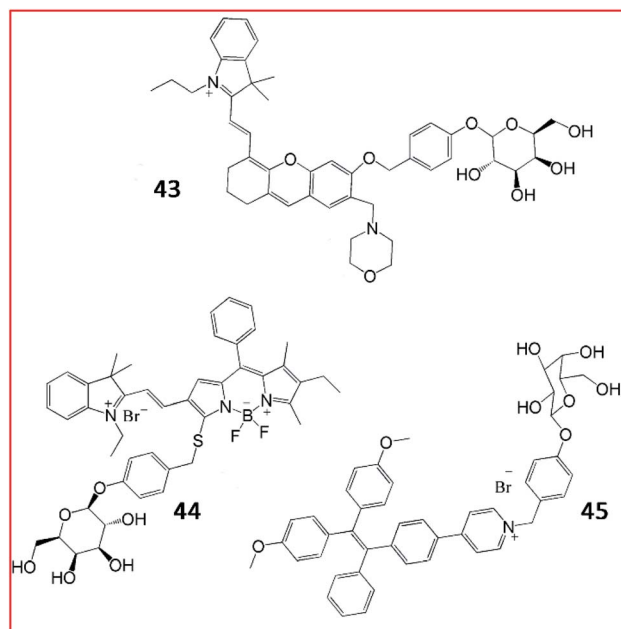**Fig. 33** The structures of fluorescent probes **43–45**. These probes were developed for the detection of β-galactosidase.

SOVK3 cancer cells and ovarian tumour tissues in nude mice.[131] Until now, probe **44** is the only reported NIR-II fluorescent probe for the detection of β-galactosidase activity.

Tang *et al.* devised an AIE-based bioimaging probe (**45**, TPE-Gal) to monitor the activity of β-galactosidase in living cells (Fig. 33). To form this tetraphenylethylene (AIEgen)-based light-up fluorescent probe, a D-galactose residue was applied as the substrate of β-galactosidase in probe **45**. Upon activation by the enzyme, the D-galactose residue left, promoting the 1, 6-elimination of p-quinone-methide, releasing the tetraphenyl-ethylene. Consequently, aggregated tetraphenyl ethylenes emitted a distinct fluorescence signal. In general, probe (**45**) displayed high specificity, good cell permeability, and high biocompatibility for the imaging of β-galactosidase in cells.[132]

3.2. Cardiovascular disease

Cardiovascular disease (CVD), a chronic disease responsible for the largest global disease burden in the world, is closely associated with age. CVD is also associated with a number of different disorders including ischaemia/reperfusion injury, ischemic heart disease, hypertension and diabetes. Many reports have indicated that overproduction of ROS is a major factor contributing to the pathogenesis of CVD due to over-loading of the capacity of antioxidants and antioxidant enzymes *in vivo*.[133,134]

Creatine kinase (CK), which catalyses the transfer of a phosphoryl group from adenosine triphosphate (ATP) to adenosine diphosphate (ADP), is closely associated with many bioenergetic processes. CK is widely expressed in many organs, such as smooth muscle, cardiac muscle, the kidney, the brain and skeletal tissue. Previous studies reported that CK expression in cells could protect against ischaemia/reperfusion injury.[135] In addition, the CK isoenzyme, CK-B is used as a biomarker of myocardial infarction. Zhang *et al.* reported a water-soluble AIE-based fluorescent probe (**46**, TPEMA) to sense the activity of CK-B (Fig. 34).[136] The inhibitor ethylmalonic acid was used as the targeting moiety to deliver the probe into the cavity of CK-B, and TPE was used as the fluorophore. When probe **46** was inserted into the cavity of CK-B, the molecular motion of TPE was restricted, and TPE emitted strong fluorescence. Altogether,
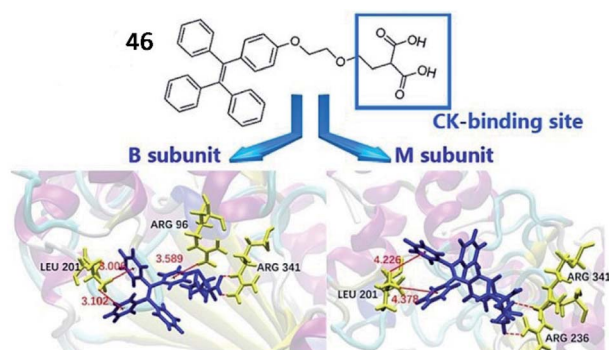

Fig. 34 The structure of probe **46** (TPEMA). Reprinted from ref. 136 with permission. Copyright 2019 Wiley-VCH.
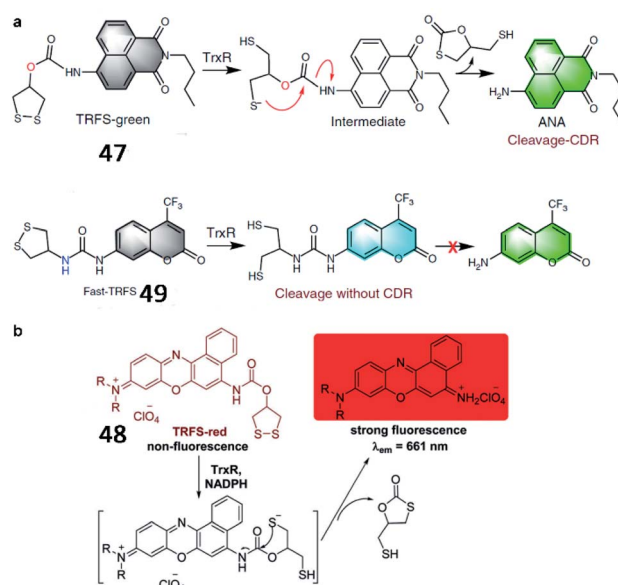

Fig. 35 (a) Reaction mechanism of **47** and **49**. Reprinted from ref. 139 with permission. Copyright 2019 Springer Nature. (b) Proposed mechanism for the activation of **48** by TrxR/NADPH. Reprinted from ref. 138 with permission. Copyright 2016 The Royal Society of Chemistry.

probe **46** displayed excellent selectivity and high sensitivity towards the CK-B subunit both in cells and *in vitro*.

Fang *et al.* developed a naphthalimide-based TrxR-activatable fluorescent probe (**47**, TRFS-green) in 2014 (Fig. 35a).[137] The probe showed green fluorescence after its cyclic disulfide scaffold was cleaved by TrxR in the presence of NADPH. **47** could be used to visualize TrxR activity in living cells and screen inhibitors of TrxR. Then, a red-emission fluorescent probe (**48**, TRFS-red) was reported by the same group (Fig. 35b).[138] The probe contained Nile blue derivative as the fluorophore and 1,2-dithiolan-4-ol as the TrxR recognition group. The maximum absorption wavelength of probe **48** was red-shifted from 530 nm to 615 nm upon activation by TrxR. Compared with the authors' previously reported probe **47** (35-fold), probe **48** possessed higher sensitivity (90-fold fluorescence enhancement) towards TrxR. Recently, the Fang group reported another new fluorescent probe (**49**, Fast-TRFS) to detect the activity of TrxR fast and specifically (Fig. 35a).[139] Based on previous work, a superfast probe was optimized, synthesized and demonstrated to exhibit 150-fold enhanced fluorescence after incubation with TrxR. More importantly, **49** displays better selectivity to TrxR than do **47** and **48**. Further mechanistic studies reveal that switching on the fluorescence of **49** is achieved by the reduction of the disulfide bond only and the process of cyclization-driven release (CDR) is not necessary, which is different from the mechanism underlying the activation of **47** or **48**. This work provides a high-throughput assay to screen for inhibitors of TrxR.

3.3. Neurodegenerative disease

Neurodegenerative diseases are a heterogeneous group of disorders caused by progressive damage to the central nervous

system. Common neurodegenerative diseases include AD, PD and Huntington's disease (HD).[140] In most neurodegenerative diseases, abundant abnormal proteins (Aβ, tau) aggregate in neural cells and extracellular compartments, affecting post-translation processing, protein solubility, and fibril formation. These aggregated proteins cannot be degraded by proteases, autophagy or the ubiquitin–proteasome system. In addition, ROS induced oxidative stress has been implicated in the exacerbation of neurodegenerative diseases.[141,142] Therefore, the development of fluorescent probes to detect ROS and ROS-associated proteins is necessary for a comprehensive understanding of the biological mechanism of ROS in neurodegenerative diseases.

3.3.1 Fluorescent probe for Aβ. To investigate the biological molecular mechanism of AD, many fluorescent probes have been developed to explore the level of aggregated Aβ in neurodegenerative diseases.[143,144] Kim *et al.* reported two fluorescent probes for the detection of Aβ plaque levels (Fig. 36). The two-photon fluorescent probe (**50**, SAD1) showed high specificity for binding Aβ plaques.[145] With a two-photon action cross-section of 170 GM, the probe could be applied to TPM imaging. In addition, probe **80** could cross the blood–brain barrier for the visualization of Aβ plaques in living mice.

Yi *et al.* reported several fluorescent probes for the detection of Aβ in AD (Fig. 36). In 2016, a spiropyran-based fluorescent probe (**51**, AN-SP) with an amino naphthalenyl-2-cyano-acrylate constituent as the targeting group for the imaging of Aβ oligomers with high affinity was developed.[146] The fluorescence of probe **51** visibly changed in the presence of Aβ oligomers. The probe could detect Aβ oligomers in both brain sections and living AD mouse models.

Many AIE-based fluorescent probes have been developed to explore aggregated Aβ. Zhu *et al.* developed an NIR AIE-based
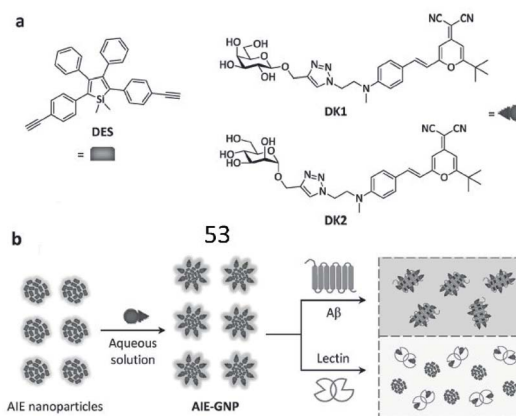

Fig. 37 (a) Structures of the AIEgen (DES) and glycoprobes (DK1 and DK2). (b) Schematic illustration of probe **53** for detection of Aβ. Reprinted from ref. 148 with permission. Copyright 2016 Wiley-VCH Verlag GmbH & Co. KGaA, Weinheim.

fluorescent probe (**52**, QM-FN-SO$_3$) for the visualization of Aβ plaques (Fig. 36).[147] This probe **52** was ultrasensitive towards Aβ plaques, owing to its remarkable binding affinity for Aβ plaques. Moreover, probe **52** could traverse the blood–brain barrier with excellent photostability. Aβ plaques in living mice were successfully visualized by probe **52**.

Tian *et al.* reported a ratiometric AIE-based fluorescent probe (**53**) for the imaging of Aβ and fibrils (Fig. 37). A silole-based AIEgen and fluorescent glycoprobes joined by supramolecular assembly constitute the probe (AIE-GNP). In the presence of Aβ, since the interaction between the AIEgen (DES) and the hydrophobic region of Aβ was stronger, Aβ could competitively bind DES and block FRET between DES and glycoprobes (Dks). The FRET efficiency between AIEgen and the glycoprobes accurately indicated the levels of Aβ and fibrils.[148]

3.3.2 Fluorescent probes for tau. Tau is a member of the microtubule-associated protein family of neuronal proteins. In neurodegenerative diseases, tau proteins are hyperphosphorylated, causing their dissociation from microtubules and aggregation to form neurofibrillary tangles in the somatodendritic compartment.[149] The longest form of tau in the human brain contains more than 80 phosphorylation sites, which can be hyperphosphorylated by protein kinases and phosphatases.[150] In neurons, insoluble aggregates of tau are integrated into membranes, which changes the membrane potential and opens voltage-gated calcium channels, inducing calcium influx. This activates NADPH oxidase, which increases ROS production, ultimately leading to oxidative stress and cell death.[151]

Several fluorescent probes have been reported to specifically bind and label tau *in vivo*. Schmidt *et al.* synthesized a set of trimethine cyanine derivative-based compounds to screen fluorescent probes for the selective imaging of tau fibrils (Fig. 38). Probes **54** could be used to visualize tau fibrils in the human AD brain and olfactory epithelium sections. These results suggest that probe **54** can target tau fibrils with a high binding rate, good aqueous solubility and low cytotoxicity.[152]
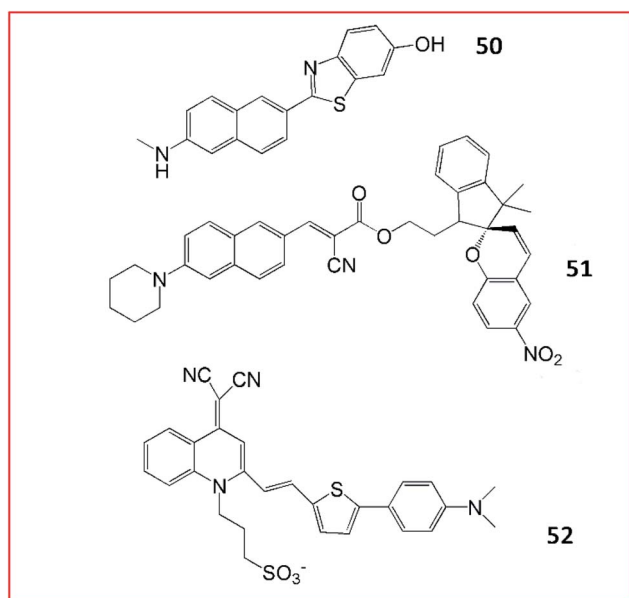

Fig. 36 The structures of probes **50–52**. These probes were developed for the detection of Aβ.
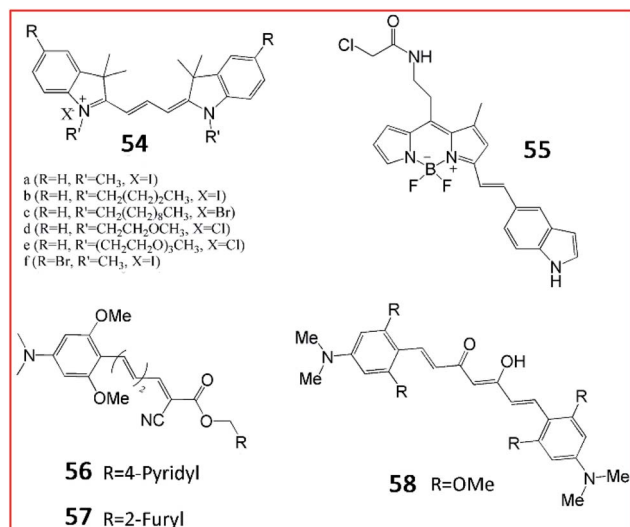
Fig. 38 The structures of probes 54–58. These probes can image tau aggregates selectively.

Fig. 39 The proposed detection mechanism of probe 59 with MAO-A. Reprinted from ref. 159 with permission. Copyright 2017 Wiley-VCH Verlag GmbH & Co. KGaA, Weinheim.

Kim *et al.* designed a BODIPY-based fluorescent probe (55, BD-tau) to observe aggregated tau in cells (Fig. 38). Probe 55 exhibited a 3.2-fold increase in fluorescence intensity in tau aggregates. Probe 55 could selectively image tau aggregates without interference from tau pre-aggregates or BSA, suggesting its high selectivity. Probe 55 could be used to detect pathological tau aggregates in live hippocampal neurons, indicating its potential for screening anti-tau aggregate drugs.[153]

NIR fluorescent probes may possess wider application in fluorescence imaging due to their deep penetration. Chong *et al.* developed NIR fluorescent probes 56 (3 g) and 57 (3 h) to identify tau fibrils in cells (Fig. 38).[154] The fluorophore curcumin was used as a fluorescent reporter in a series of probes with a novel donor–π–acceptor architecture. The fluorescence properties of these probes were evaluated. Upon mixing with tau, the probe 56 and 57 exhibited large Stoke shifts with emission at 650 nm. In addition, probes 56 and 57 evoked brighter fluorescence towards tau aggregates over Aβ fibrils, suggesting that probes 56 and 57 possessed high selectivity.[74] The authors also reported a curcumin-based NIR fluorescent probe (58) for the imaging of tau fibrils in 2015.[155] A curcumin derivative was chosen as the fluorescent reporter and tau fibril-specific binding group. Intense fluorescence was observed upon mixing with tau fibrils, confirming its higher binding affinity for pre-aggregated tau.

3.3.3 Fluorescent probes for monoamine oxidases. Monoamine oxidases (MAOs, EC 1.4.3.4), which include two isozymes in mammalian tissues, MAO-A and MAO-B, are a family of enzymes that catalyse the oxidative deamination of monoamines. MAO catalysis requires flavin adenine dinucleotide (FAD) as a cofactor. In addition, ROS are simultaneously produced when MAOs catalyse the transformation of biogenic amines to aldehydes. Over-activation of MAOs in brain tissues increases the level of ROS, which leads to oxidative stre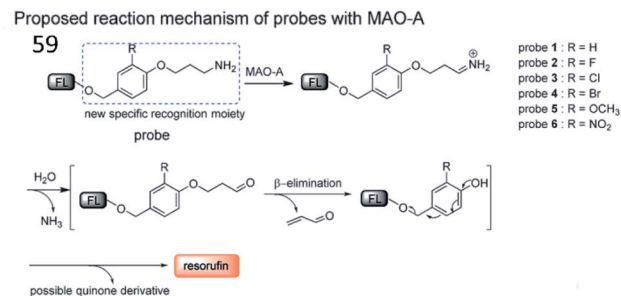ss and eventually promotes the occurrence and development of neurodegenerative diseases.[156] Both MAO-A and MAO-B exist in neuronal cells and astrocytes, and their substrate specificities are different. The preferable substrate of MAO-A was serotonin (5-hydroxytryptamine, 5-HT), while MAO-B showed higher affinity towards benzylamine and phenylethylamine.[157,158]

Inspired by the characteristic structures of MAO-A inhibitors, Ma *et al.* reported a strategy to design and synthesize a fluorescent probe (59) for the specific imaging of MAO-A (Fig. 39). Based on this strategy, the structure (*i.e.* phenol with different substituents) of clorgyline (the specific inhibitor of MAO-A) was combined with propylamine, a new specific recognition unit for MAO-A, connected to the fluorophore resorufin.[159] In the presence of MAO-A, the amino group in the probe was oxidized to imine and underwent deamination to form an aldehyde. Then, the propionaldehyde was removed by a β-elimination reaction, and the substituted phenol was removed by 1,6-rearrangement elimination, ultimately releasing resorufin. Altogether, probe 59 possesses the highest specificity for the detection of MAO-A and can distinguish between MAO-A and MAO-B.

Many two-photon fluorescent probes have been reported to detect the activities of MAOs. Kim *et al.* developed a two-photon probe (60, PCP-1) for the specific targeting and imaging of MAO-A (Fig. 40). This probe consisted of a rhodamine derivative as a two-photon fluorescent group and an MAO-A-selective inhibitor (moclobemide) as a specific recognition. The probe targeted and bound MAO-A through a selective inhibitor of MAO-A and could monitor MAO-A in cancer cells. In addition, probe 60 prevented the proliferation and metastasis of cancer cells by inhibiting the activity of MAO-A.[160]
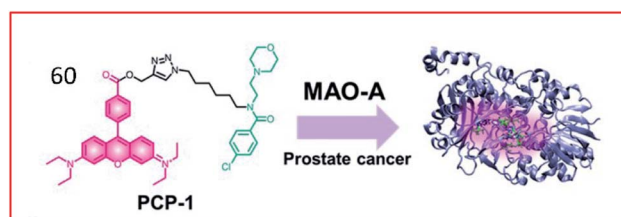

Fig. 40 Design of probe 60 targeting MAO-A for the detection of prostate cancer. Reprinted from ref. 160 with permission. Copyright 2019 The Royal Society of Chemistry.
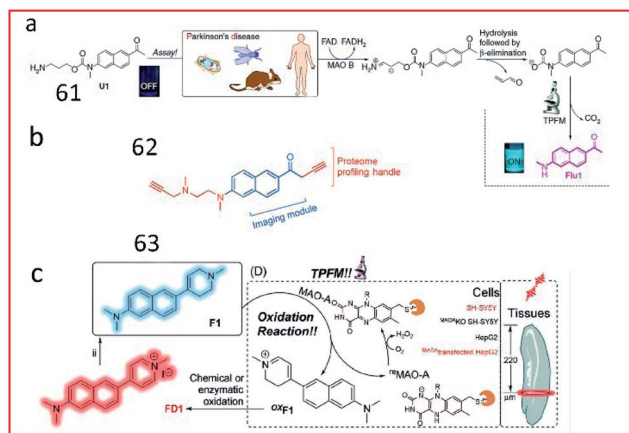
Fig. 41 Overview of the design and synthesis of MAO-specific probes. (a) **61**. Reprinted from ref. 161 with permission. Copyright 2014 Macmillan Publishers Limited. (b) **62**. Reprinted from ref. 162 with permission. Copyright 2015 Wiley-VCH Verlag GmbH & Co. KGaA, Weinheim. (c) **63**. Reprinted from ref. 163 with permission. Copyright 2020 Wiley-VCH Verlag GmbH & Co. KGaA, Weinheim.

Fig. 42 The structure of probe **64**. Reprinted from ref. 164 with permission. Copyright 2020 American Chemical Society.

Yao *et al.* reported the first two-photon enzyme probe (**61**, U1) for the specific detection of MAO-B activity (Fig. 41a).[161] Probe **97** contained a 2-methylamino-6-acetylnaphthalene (acedan) moiety as the fluorophore and a propylamine moiety as a reactive group specific for MAO-B. Initially, due to the PeT process between acedan and the adjacent carbamate, the fluorescence of acedan was quenched. In the presence of MAO-B, the amino group was oxidized to an aldehyde group (*via* an imine intermediate), and propionaldehyde and CO_2 were spontaneously released through β-elimination. Then, free Flu1 was released, emitting strong fluorescence based on blockade of the PeT effect. This probe could detect the activity of MAO-B in biological samples with high sensitivity and specificity. In 2015, by combining the fluorophore of probe U1 with the proteome profiling handle of the previously reported proteome-profiling-enabled probe P3, the authors further described a new activity-based dual-purpose probe (**62**, M2) for the detection of MAO-B activity (Fig. 41b).[162] Probe **62** can detect endogenous MAO-B activity *via in situ* proteome profiling and live-cell imaging. Furthermore, this probe could detect the activity of MAO-B in established PD models.

Based on this work, the structure of naphthalene in probe U1 was retained by exchanging the positions of the propylamine warhead and fluorophore, and combined with *N*-alkylated tetrahydropyridine to obtain the first MAO-A-specific two-photon fluorescent probe (**63**, F1) (Fig. 41c).[163] In the presence of MAO-A, the probe was oxidized to oxF1, and then transformed to FD1 through chemical or enzymatic oxidation in the system. Subsequently, the tetrahydropyridine group in probe **63** was oxidized to pyridine, which had strong electron-withdrawing ability, leading to increased fluorescence based on an enhanced push–pull electron effect. Probe **63** was successfully used to detect MAO-A activity in fresh mouse/human brain and tumour tissues. Probes **61**–**63** reported by Yao[161–163] and co-workers
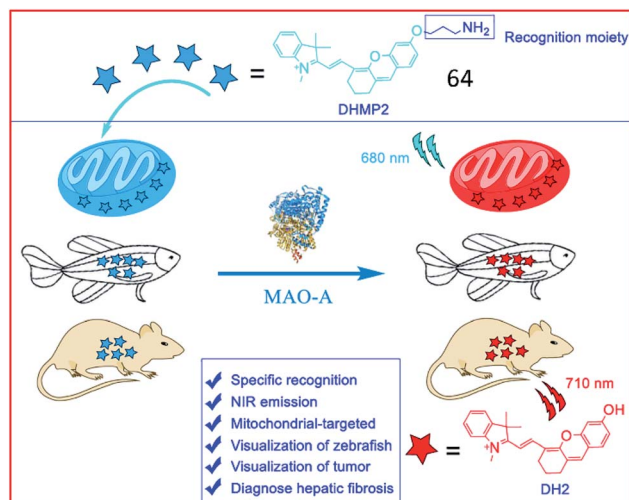
possess excellent selectivity towards MAO-B or MAO-A and are powerful tools for PD diagnosis.

Several NIR MAO-activatable fluorescent probes were designed. Qin *et al.* created four mitochondrial-targeted dihydroxanthene (DH)-derived NIR fluorescent probes, DHMP1–4, for the detection of MAO-A; among these probes, probe **64** (DHMP2) was the most efficacious (Fig. 42). Probe **64** contained a dihydroxanthene group as the fluorophore, a propylamine group as the MAO-A reaction unit, and a tetramethyl-indole cation group as a mitochondrial targeting group. Upon cleavage by MAO-A, the hydroxyl group of the probe was exposed, restoring fluorescence. Probe **64** was used to monitor MAO-A activity in cellular mitochondria, zebrafish and tumour-bearing nude mice.[164]

To simultaneously image the activity of MAO-B and the generation of ROS, Chen and co-workers developed two NIR ratiometric fluorescent probes, probes **65** (MitoHCy-NH$_2$) and **66** (MitoCy-NH$_2$) (Fig. 43). In the presence of MAO-B, conversion of the amino group to an imine intermediate catalysed by MAO-B was accompanied by the generation of ROS, and the reduced fluorophore in probe **65** was oxidized by ROS to restore fluorescence. Subsequently, the absence of the propylamine group
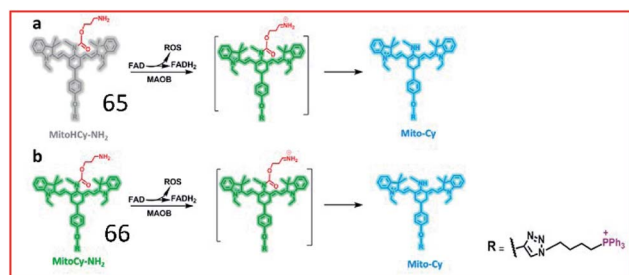

Fig. 43 Molecular structures and the proposed detection mechanism of **65** and **66**. Reprinted from ref. 165 with permission. Copyright 2018 American Chemical Society.
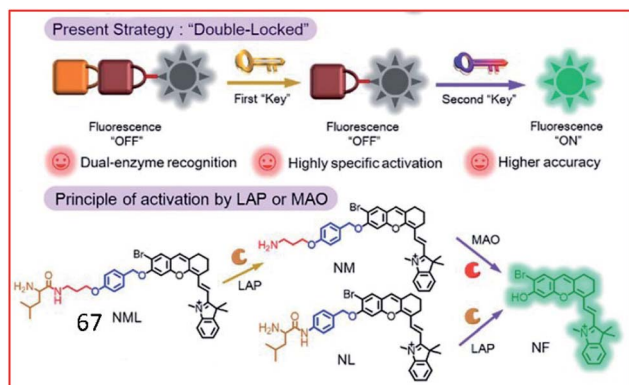
Fig. 44 Design strategy of the enzyme–activated molecular probe **67**. Reprinted from ref. 166 with permission. Copyright 2019 The Royal Society of Chemistry.

caused β-elimination, leading to blue-shifting of the fluorescence maximum emission wavelength of the probe. Therefore, probes **65** and **66** can be used for the synchronous detection of MAO-B and ROS in cell and aging mouse models.[165]

Recently, a double-locked strategy was used to design a fluorescent probe. Zhang *et al.* designed a double-locked probe (**67**, NML) for the detection of LAP and MAO activities (Fig. 44). Probe **67** contained leucine, propylamine and an NIR fluorophore (NF). The leucine was connected to the amino group of propylamine through a pseudo-peptide bond, and the other end of the propylamine was incorporated into NF with an elimination-type spacer (*para*-hydroxybenzyl group). In the presence of LAP and MAO, the pseudo-peptide bond between the leucine and propylamine groups was cleaved by LAP, and the exposed amino group was oxidized by MAO, which further caused a β-elimination reaction and released the NF. Probe **67** could distinguish normal, drug liver injury and cirrhotic mice by detecting the activities of LAP and MAO in the serum.[166]

3.3.4 Fluorescent probes for acetylcholinesterase. Acetylcholine (ACh) is a key neurotransmitter in the nervous system that can transmit messages from nerve cells to other cells. The level of ACh in the brain has a direct correlation with the progression of neurodegenerative diseases, such as AD and
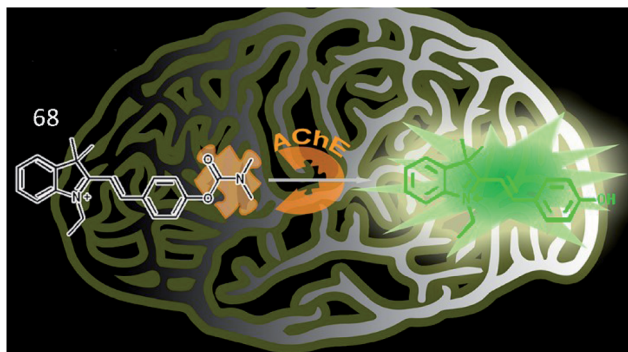

Fig. 45 Recognition mechanism of probe **68** and structure of MCYO. Reprinted from ref. 168 with permission. Copyright 2019 American Chemical Society.
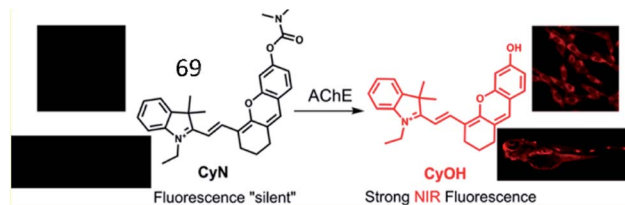

Fig. 46 Proposed recognition mechanism for **69** sensing AChE. Reprinted from ref. 169 with permission. Copyright 2019 American Chemical Society.

depression. Acetylcholinesterase (AChE, EC:3.1.1.7) is a kind of hydrolase enzyme that catalyses the hydrolysis of ACh into acetate and choline, resulting in the accelerated production of Aβ to form amyloid fibrils. Inhibiting the activity of AChE was shown to be an effective therapeutic strategy for AD. Therefore, various methods to detect AChE and screen for inhibitors have been established.[167]

Tang *et al.* synthesized a two-photon fluorescence probe (**68**, MCYN) that contained merocyanine as a fluorophore and dimethyl carbamate as an enzymatic recognition unit for the real-time detection of AChE activity (Fig. 45).[168] When AChE catalysed the cleavage of the dimethyl carbamate group in probe **68**, MCYO was produced, accompanied by an enhanced push–pull electron effect, causing the emission of bright fluorescence. Probe **68** was successfully employed to sensitively and selectively monitor AChE activity in living cells and in the brains of mice with depression. This work also suggested that the $O_2^{\cdot-}$ level is positively correlated with AChE activity in depression.

Based on this work, Guo *et al.* developed an NIR "turn-on" fluorescent sensor (**69**, CyN) consisting of an *N,N*-dimethyl carbamyl moiety as the AChE recognition substrate and hemicyanine as the fluorescent reporter for the highly selective detection of the AChE (Fig. 46).[169] Upon cleavage of the carbamyl group by AChE, probe **69** was transformed into a hemicyanine dye (CyOH). The fluorescence intensity of the probe was distinctly enhanced due to the push–pull electron effect in CyOH. This probe was used to monitor changes in AChE activity in cells and in zebrafish.

Furthermore, many other NIR fluorescence sensors and FRET-based nano probes were also developed to sense the activity of AChE.[170,171] For instance, Qian *et al.* assembled a fluorescence nanoprobe, polycytosine-templated silver nanoclusters (dC_{12}–Ag NCs), for the ultrasensitive tracking of AChE activity.[172] Hu *et al.* exploited a carbon dot (CD)-based ratiometric fluorescence sensor to track AChE and butyrylcholinesterase (BChE) activities.[173]

3.4. Fibrotic disease

Fibrosis is frequently associated with many chronic inflammatory diseases, such as cardiomyopathy, diabetes, obesity, pneumonia and liver diseases. The excessive accumulation of fibrous connective tissues around damaged tissue leads to scarring, organ dysfunction, death, and diseases including renal fibrosis, idiopathic pulmonary fibrosis (IPF) and liver

fibrosis.[174] ROS play an essential role in fibrosis by their involvement in the TGF-β1 signalling pathway and post-transcriptional and epigenetic mechanisms. Although many immunological and molecular mechanisms contribute to the progression of fibrotic disease, specific biomarkers to identify disease and evaluate the effect of therapy are lacking.[175] Therefore, it is highly important to develop fast, specific fluorescent probes to sense biomarkers of fibrotic diseases in real time.

3.4.1 Fluorescent probes for fibroblast activation protein. Fibroblast activation protein (FAP, EC 3.4.2.1.B28) is a membranous glycoprotein among serine proteases of the prolyl oligopeptidase gene family. FAP participates in fibrosis, extracellular matrix degradation, tissue remodelling, inflammation and tumour growth.[176] FAP expression is scarce in healthy tissues, but FAP is overexpressed in tissue modelling, fibrotic diseases and tumours. Furthermore, FAP was shown to be involved in extracellular matrix remodelling and collagen clearance, especially in mouse models of IPF.[177] In addition, ROS play an essential role in fibroblast activation.[178] Therefore, many studies have been performed to develop FAP specific fluorescent probes for the detection of FAP in various biological processes.[179,180]

Li *et al.* reported a bioluminogenic probe (**70**) for the imaging of FAP *in vivo* and screening of FAP inhibitors *in vitro*.[181] *N*-Carbobenzyloxy–Gly–Pro–OH (Cbz–Gly–Pro–OH) served as the FAP substrate in this probe (Fig. 47). When the substrate of firefly luciferase, aminoluciferin, was caged by Cbz–Gly–Pro–OH, the bioluminescence of probe **70** was undetectable. After being released by FAP, the probe generated bioluminescence *via* the reaction between aminoluciferin and firefly luciferase. Probe **70** showed a 185-fold increase in bioluminescence upon the addition of 500 ng mL^{-1} FAP. With an extremely low detection limit of 0.254 ng mL^{-1}, probe **70** was used to evaluate the activity of FAP with high selectivity and sensitivity in living mice.

Recently, a series of NIR fluorescent probes for the detection of FAP were developed. Pu *et al.* reported an NIR fluorescent probe (**71**, FNP1) that could be activated by FAPa to image keloid and skin cells (Fig. 48).[182] This probe consisted of a CyOH as the fluorophore and a carbobenzyloxy–Gly–ProOH (Cbz–Gly–Pro) as

Fig. 48 Design and mechanism of **71** for FAP imaging. Reprinted from ref. 182 with permission. Copyright 2018 Wiley-VCH.
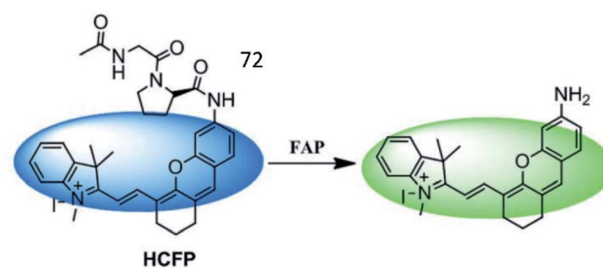
Fig. 49 Mechanism of the probes **72** for FAP imaging. Reprinted from ref. 183 with permission. Copyright 2018 The Royal Society of Chemistry.

a reactive group specific for FAPa. These two moieties were linked by a carbamate-based self-immolative moiety. With the addition of FAPa, the substrate and the self-immolative moiety were cleaved; therefore, CyOH, which contained a free hydroxyl group, emitted bright fluorescence. Due to its beneficial high selectivity and sensitivity towards FAPa, probe **71** can distinguish keloid cells from other normal skin cells, allowing it to detect abnormal scar fibrous lesions at an early stage.

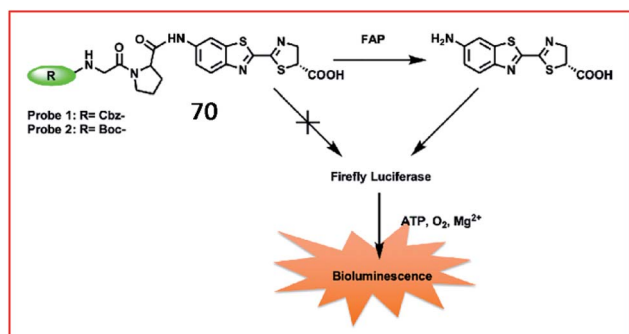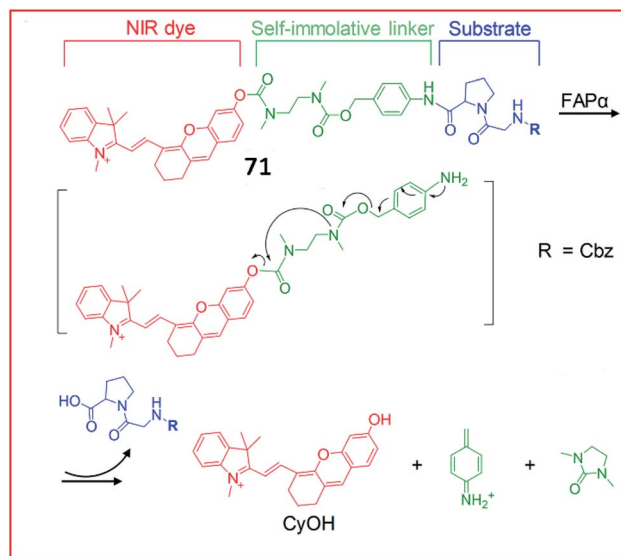**Fig. 47** Design strategy for the probes **70** of FAP. Reprinted from ref. 181 with permission. Copyright 2019 American Chemical Society.

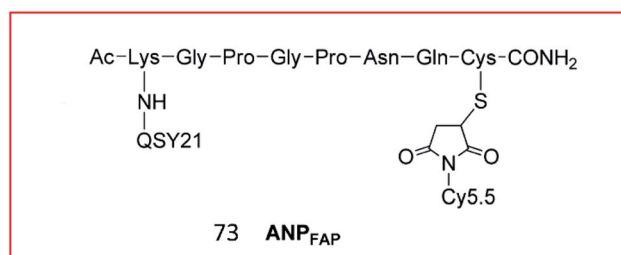**Fig. 50** Structure of probe **73** for FAP imaging. Reprinted from ref. 184 with permission. Copyright 2012 American Chemical Society.

Wu *et al.* developed a hemicyanine-based FAP-activatable NIR fluorescent probe (**72**, HCFP) consisting of hemicyanine as the fluorophore and a dipeptide derivative as the recognition group for FAP (Fig. 49).[183] In the presence of FAP, the amide bond was cleaved, releasing the amino fluorophore, which exhibited strong fluorescence. Probe **72** possesses good selectivity and sensitivity for cancer cell detection *via in vitro* and *in vivo* imaging.

Cheng *et al.* explored a FRET-based NIR fluorescence probe (**73**, APNFAP) for the detection of FAPα *in vivo* (Fig. 50). Probe **73** consisted of an NIR dye (Cy5.5) and a quenching dye (QSY21) linked by a FAPα-specific peptide substrate (KGPGPNQC). Due to the FRET effect between Cy5.5 and QSY21, the fluorescence of probe **73** was initially quenched. Upon cleavage by FAPα, the specific peptide bond was broken, causing the release of Cy5.5, which emitted bright fluorescence. Probe **73** was applied to label FAPα-positive tumour cells with high selectivity *in vivo*.[184]

3.4.2 Fluorescent probes for glutathione S-transferases.

The glutathione S-transferases (GSTs, EC 2.5.1.18) are a family of protein isozymes involved in phase II metabolism that can eliminate ROS and catalyse the conjugation of glutathione (GSH) to numerous hazardous xenobiotics.[185] There are three superfamilies of GSTs: cytosolic GSTs (including 13 classes of GSTs: alpha, beta, delta, epsilon, zeta, theta, mu, nu, pi, sigma, tau, phi, and omega), mitochondrial GSTs, and microsomal GSTs. GSTs play crucial roles in IPF, hepatic fibrosis, hormone biosynthesis, peroxide breakdown and dehydroascorbate reduction.[186]

Nagano *et al.* designed and synthesized the first GST fluorescent probe **74**.[187] The probe was composed of a xanthene group as a fluorophore and 3,4-dinitrobenzanilide (NNBA) as an enzyme-recognition site (Fig. 51). Probe **74** contained a hydrophilic carboxyl group that could detect GST activity in recombinant cells and lysates *in vitro*. To improve permeability, a lipophilic methyl group was introduced into probe **75**. Therefore, **75** allowed good optical characterization to detect GST in living cells. In the presence of GST, GST catalysed GSH to replace the nitro group on the 5-position carbon in NNBA, enhancing fluorescence *via* blockade of the PeT process. Therefore, probe **74** can be used for high-throughput screening
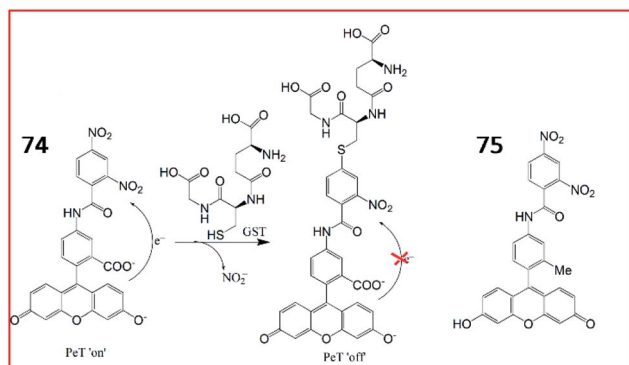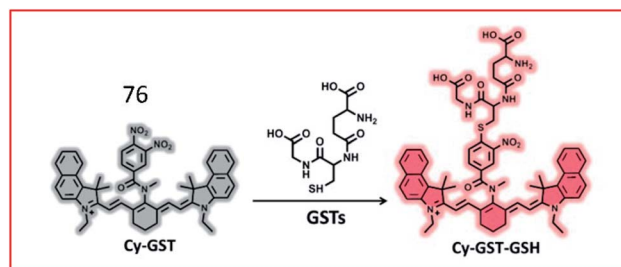
Fig. 52 Proposed detection mechanism of the probe **76** against GSTs. Reprinted from ref. 188 with permission. Copyright 2019 American Chemical Society.

of GST inhibitors, and probe **75** can be applied to detect GST activity in live cells with high spatiotemporal resolution.

Lv *et al.* developed an "off–on" switch NIR fluorescent probe (**76**, Cy-GST) for the detection of GSTs (Fig. 52). Cy-GST contained a specific substrate of human GST (3,4-dinitrobenzanilide moiety) as the specific response group, and a benzoheptamethine cyanine dye as the fluorescent reporter group. The fluorescence of the probe was quenched due to PeT between the fluorophore and the strong electron-withdrawing 3,4-dinitrobenzanilide moiety. In the presence of GSTs, GSTs catalysed the binding of glutathione to probe **76**, resulting in the sulfhydryl substitution derivative Cy-GST-GSH. Glutathionylation of probe **76** blocked the PeT process and restored the fluorescence. Probe **76** was used to detect GST in cells and IPF mouse models with high selectivity.[188]

3.5. Infectious diseases and inflammation diseases

Viruses, bacteria, and parasites comprise a vast group of aetiological agents that cause acute or chronic diseases and inflammation in humans. ROS have been implicated in several infectious diseases by inducing the assembly and activation of inflammasomes, which are multiprotein cytoplasmic complexes involved in innate immune signaling pathways in response to various pathogens and injury. Numerous proteins participate in intracellular immune-related signaling pathways and have the potential to be biomarkers or drug targets in the future. Recently, many fluorescent probes to sense the expression levels or activities of inflammatory proteins have been reported.[189]

The leukotriene A_4 hydrolase (LTA$_4$H, EC 3.3.2.6) is a cytosolic dual-function enzyme that catalyses the hydrolysis of leukotriene A_4 (LTA$_4$) to form the proinflammatory mediator leukotriene B_4 (LTB$_4$). As a chemoattractant and stimulator that

Fig. 51 The structures of probe **74** and **75**, and GST-catalyzed glutathionylation of **74**.
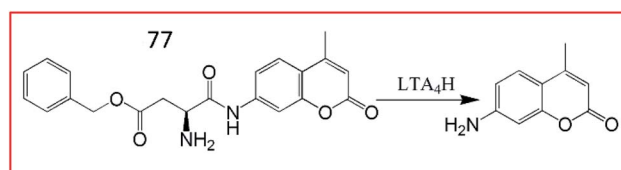
Fig. 53 Schematic illustration of probe **77** for the detection of LTA$_4$H.

induces ROS generation in macrophages, neutrophils, T-cells, and other fibroblasts, LTB$_4$ is involved in many human pathologies, such as chronic obstructive pulmonary disease, inflammatory bowel disease, rheumatoid arthritis, asthma, and connective tissue disease.[190,191] Therefore, LTA$_4$H is believed to participate in inflammatory progression by the biosynthesis of LTB$_4$, which suggests that the development of fluorescent probes targeting LTA$_4$H may contribute to drug discovery.

In 2018, Tang *et al.* discovered a small molecular fluorescent probe (**77**, ASPC) for the detection of LTA$_4$H. This novel two-photon fluorescent probe (**77**) incorporated the substrate of LTA$_4$H (unnatural amino acid L-AspBzl) into the fluorophore 7-amino-4-methylcoumarin (AMC) (Fig. 53).[192] The amide bond between AMC and L-AspBzl in probe **77** could be recognized and broken by LTA$_4$H, inducing bright green fluorescence under two-photon excitation at 690 nm. Probe **77** was capable of monitoring the activity of LTA$_4$H in lipopolysaccharide-stimulated cells by one-photon and two-photon fluorescence imaging. Moreover, this probe could identify inflamed lung tissues by imaging LTA$_4$H.

To obtain deeper tissue penetration, a fluorescent and photoacoustic dual-mode imaging probe (**78**, Cy-ASP) was developed by the same group in 2019 (Fig. 54).[193] The NIR fluorophore hemicyanine (Cy-NH$_2$) was chosen as the fluorescent and photoacoustic signal reporter, and L-AspBzl was used as the recognition site for LTA$_4$H. Probe **78** could visualize LTA$_4$H at inflammatory sites without dissection *via* fluorescence and photoacoustic dual-model imaging.
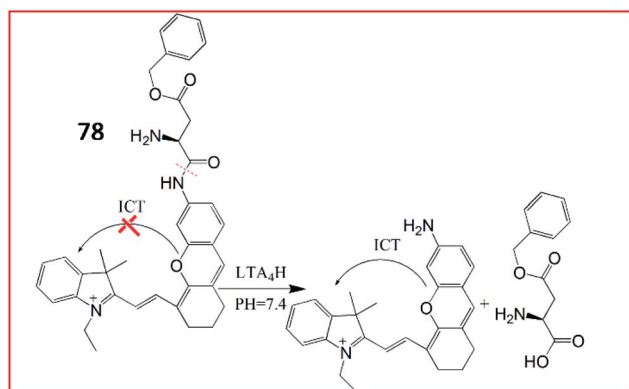
Human neutrophil elastase (NE) is a single chain glycoprotein consisting of 267 amino acids belonging to the serine protease family.

When inflammation occurs, neutrophils are recruited to the inflammatory site, where they release the toxic molecules NE and ROS, leading to tissue destruction at the inflammatory site. Many studies have shown that a rise in NE levels is related to a variety of inflammatory diseases, especially chronic obstructive pulmonary disease, and acute lung injury. Yang *et al.* reported several fluorescent sensors to detect the activity of NE. The first non-peptide-based fluorescent probe that they developed (**79**) contained a 7-amino-4-trifluoromethyl coumarin group as the fluorophore and a pentafluoro-propionyl group as the quencher (Fig. 55a).[194] The amide bond between the fluorophore and quencher was the reaction site for human NE. Specific cleavage of the amide bond in the probe by NE strongly enhances fluorescence. In 2019, the authors further presented an NIR fluorescent probe (**80**, NEP), which was based on a small-molecule substrate, for the detection of NE (Fig. 55b). Probe **80** consisted of a pentafluoroethyl moiety as the recognition unit and a hemicyanine dye moiety as the fluorophore. In the presence of NE, cleavage of the amide bond by NE restored the ICT process, inducing the strong NIR fluorescence of hemicyanine dye. Probe **80** was applied for the real-time monitoring of NE activity in an acute kidney injury (ALI) mouse model.[195]

4. Conclusions

The expression levels and activities of proteins are closely related to numerous metabolic processes, which are accompanied by oxidative stress to varying degrees, in living organisms. The cooperation between proteins and ROS affects the occurrence and development of diseases *via* either ROS-regulating proteins or ROS control by proteins. Thus, a thorough understanding of the expression levels and activities of ROS-associated proteins may promote defining the pathogenesis of diseases and accelerate drug development. In this review, we illustrate the strategies of fluorescent probe design and sensing mechanisms of fluorescent probes to identify these proteins with or without catalytic activity and summarize the advances in the imaging of these proteins in different diseases with typical probes made over the past decade. Even so, as some challenges for the accurate *in situ* detection of ROS-associated proteins remain, the following considerations are suggested:

(1) Highly sensitive fluorescent probes for *in situ* monitoring of the dynamic ROS modification of proteins should be created. To date, ROS modification patterns and protein sites are usually investigated by mass spectrometry *in vitro*. However, this method cannot accurately evaluate the concentrations of ROS and proteins in living cells and neglects upstream and downstream regulation. Given that native conditions are absent, this *in vitro* method can only partially indicate the interaction between ROS and proteins. Therefore, one major issue that needs to be addressed is how to exploit novel fluorescent probes to examine the ROS modification patterns of proteins in real time.

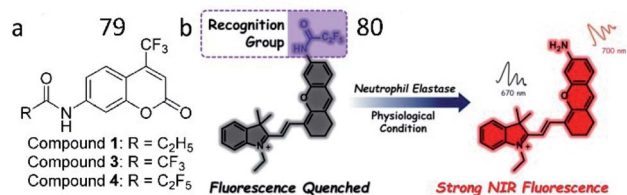**Fig. 54** Sensing mechanism of probe **78** for the detection of LTA$_4$H.

Fig. 55 (a) The structure of probe **79**. Reprinted from ref. 194 with permission. Copyright 2013 American Chemical Society. (b) Sensing mechanism of probe **80** for NE. Reprinted from ref. 195 with permission. Copyright 2019 American Chemical Society.

(2) New probes with deeper signal penetration are needed. Optical penetration depths limit the clinical application of existing fluorescent probes, such as NIR probes whose penetration is still shallow at approximately 1 mm. The following strategies are selected as possible solutions. First, NIR fluorescent probes whose emission wavelengths are 1500–1700 nm may be improved tools due to their deep penetration (10 mm), low level of photo-scattering, and nearly absent autofluorescence.[196] Second, PAI probes can provide images at a high spatial resolution from deep tissues through the combination of optical and ultrasonic signals. Third, CRET-based NIR fluorescent probes without an additional light source are promising for deep tissue imaging applications.[197]

(3) The probe response time should be improved. Low substrate specificity and the high degree of steric hindrance due to the probe seriously impede enzymatic reactions, leading to extended probe response times towards the target enzyme. To raise the reaction rate, screening novel specific substrates with low Michaelis constant might be helpful.

(4) The simultaneous detection of multiple proteins is needed. In living organisms, multiple proteins synchronously regulate cellular processes; however, traditional approaches still require extensive efforts to verify the undefined roles of some proteins in signalling networks. Using new probes with high selectivity and sensitivity, multicolour *in situ* fluorescence imaging will provide convincing evidence to reveal how various ROS-associated proteins are implicated in diseases.

(5) Diagnosis and therapy should be integrated. Based on the roles of ROS-associated proteins in diseases, multifunctional fluorescent probes could not only diagnose various diseases in real time by fluorescence imaging but also facilitate the use of suitable treatments.[198] To further improve efficiency, theranostic agents might have other applications, such as MRI, drug delivery, and PDT/PTT.

Author contributions

Hui Wang was the main author of the review, and completed the collection and analysis of relevant literature and the writing of the first draft of the paper. Xin Wang and Mingyan Dong participated in the analysis and collation of literature; Ping Li, Shao Q. Yao, Bo Tang were the originators and principals of the review, who directed the writing of the paper. The final text was read and agreed upon by all authors.

Conflicts of interest

There are no conflicts to declare.

Acknowledgements

Notes and references

1 C. A. Ross and M. A. Poirier, *Nat. Med.*, 2004, **10**(Suppl), S10–S17.
2 J. P. Taylor, J. Hardy and K. H. Fischbeck, *Science*, 2002, **296**, 1991–1995.
3 H. W. Liu, L. Chen, C. Xu, Z. Li, H. Zhang, X. B. Zhang and W. Tan, *Chem. Soc. Rev.*, 2018, **47**, 7140–7180.
4 J. Zhang, X. Chai, X. P. He, H. J. Kim, J. Yoon and H. Tian, *Chem. Soc. Rev.*, 2019, **48**, 683–722.
5 R. A. Cairns, I. S. Harris and T. W. Mak, *Nat. Rev. Cancer*, 2011, **11**, 85–95.
6 O. C. Olson and J. A. Joyce, *Nat. Rev. Cancer*, 2015, **15**, 712–729.
7 L. M. Coussens, B. Fingleton and L. M. Matrisian, *Science*, 2002, **295**, 2387–2392.
8 A. Martinez, M. Portero-Otin, R. Pamplona and I. Ferrer, *Brain Pathol.*, 2010, **20**, 281–297.
9 H. Xiao, W. Zhang, P. Li, W. Zhang, X. Wang and B. Tang, *Angew Chem. Int. Ed. Engl.*, 2020, **59**, 4216–4230.
10 K. Brieger, S. Schiavone, F. J. Miller and K. H. Krause, *Swiss Med. Wkly.*, 2012, **142**, w13659.
11 A. Popa-Wagner, S. Mitran, S. Sivanesan, E. Chang and A. M. Buga, *Oxid. Med. Cell. Longevity*, 2013, **2013**, 963520.
12 D. H. F. H. B, *Biomarkers*, 1997, **2**, 117–123.
13 X. Zhang, Y. Xiao and X. Qian, *Angew Chem. Int. Ed. Engl.*, 2008, **47**, 8025–8029.
14 D. Wu, A. C. Sedgwick, T. Gunnlaugsson, E. U. Akkaya, J. Yoon and T. D. James, *Chem. Soc. Rev.*, 2017, **46**, 7105–7123.
15 L. Qian, L. Li and S. Q. Yao, *Acc. Chem. Res.*, 2016, **49**, 626–634.
16 J. Li, J. Wang, H. Li, N. Song, D. Wang and B. Z. Tang, *Chem. Soc. Rev.*, 2020, **49**, 1144–1172.
17 J. Mei, N. L. Leung, R. T. Kwok, J. W. Lam and B. Z. Tang, *Chem. Rev.*, 2015, **115**, 11718–11940.
18 Y. Hong, J. W. Lam and B. Z. Tang, *Chem. Soc. Rev.*, 2011, **40**, 5361–5388.
19 J. D. Zhang, J. Mei, X. L. Hu, X. P. He and H. Tian, *Small*, 2016, **12**, 6562–6567.
20 H. Shi, J. Liu, J. Geng, B. Z. Tang and B. Liu, *J. Am. Chem. Soc.*, 2012, **134**, 9569–9572.
21 H. Tong, K. Lou and W. Wang, *Acta Pharm. Sin. B*, 2015, **5**, 25–33.
22 F. Chiti and C. M. Dobson, *Annu. Rev. Biochem.*, 2006, **75**, 333–366.
23 W. M. Chang, M. Dakanali, C. C. Capule, C. J. Sigurdson, J. Yang and E. A. Theodorakis, *ACS Chem. Neurosci.*, 2011, **2**, 249–255.
24 C. H. Heo, K. H. Kim, H. J. Kim, S. H. Baik, H. Song, Y. S. Kim, J. Lee, I. Mook-jung and H. M. Kim, *Chem. Commun.*, 2013, **49**, 1303–1305.

25 C. H. Heo, A. R. Sarkar, S. H. Baik, T. S. Jung, J. J. Kim, H. Kang, I. Mook-Jung and H. M. Kim, *Chem. Sci.*, 2016, **7**, 4600–4606.

26 J. Zhang, X. Wang, V. Vikash, Q. Ye, D. Wu, Y. Liu and W. Dong, *Oxid. Med. Cell. Longevity*, 2016, **2016**, 4350965.

27 L. Tochhawng, S. Deng, S. Pervaiz and C. T. Yap, *Mitochondrion*, 2013, **13**, 246–253.

28 V. Sosa, T. Moline, R. Somoza, R. Paciucci, H. Kondoh and M. E. LLeonart, *Ageing Res. Rev.*, 2013, **12**, 376–390.

29 G. Y. Liou and P. Storz, *Free Radic. Res.*, 2010, **44**, 479–496.

30 M. Poreba, A. Strozyk, G. S. Salvesen and M. Drag, *Cold Spring Harbor Perspect. Biol.*, 2013, **5**, a008680.

31 Z. Su, Z. Yang, Y. Xu, Y. Chen and Q. Yu, *Mol. Canc.*, 2015, **14**, 48.

32 S. J. Riedl and Y. Shi, *Nat. Rev. Mol. Cell Biol.*, 2004, **5**, 897–907.

33 R. S. Hotchkiss and D. W. Nicholson, *Nat. Rev. Immunol.*, 2006, **6**, 813–822.

34 X. H. Cao, A. H. Wang, C. L. Wang, D. Z. Mao, M. F. Lu, Y. Q. Cui and R. Z. Jiao, *Chem. Biol. Interact.*, 2010, **183**, 357–362.

35 J. H. Kim, S. Y. Lee, S. Y. Oh, S. I. Han, H. G. Park, M. A. Yoo and H. S. Kang, *Oncol. Rep.*, 2004, **12**, 1233–1238.

36 T. I. Kim, H. Jin, J. Bae and Y. Kim, *Anal. Chem.*, 2017, **89**, 10565–10569.

37 D. Ye, A. J. Shuhendler, L. Cui, L. Tong, S. S. Tee, G. Tikhomirov, D. W. Felsher and J. Rao, *Nat. Chem.*, 2014, **6**, 519–526.

38 M. Hu, L. Li, H. Wu, Y. Su, P. Y. Yang, M. Uttamchandani, Q. H. Xu and S. Q. Yao, *J. Am. Chem. Soc.*, 2011, **133**, 12009–12020.

39 O. Julien and J. A. Wells, *Cell Death Differ.*, 2017, **24**, 1380–1389.

40 S. Y. Li, L. H. Liu, H. Cheng, B. Li, W. X. Qiu and X. Z. Zhang, *Chem. Commun.*, 2015, **51**, 14520–14523.

41 L. E. Edgington, A. B. Berger, G. Blum, V. E. Albrow, M. G. Paulick, N. Lineberry and M. Bogyo, *Nat. Med.*, 2009, **15**, 967–973.

42 T. I. Kim, H. Jin, J. Bae and Y. Kim, *Anal. Chem.*, 2017, **89**, 10565–10569.

43 W. Liu, S. J. Liu, Y. Q. Kuang, F. Y. Luo and J. H. Jiang, *Anal. Chem.*, 2016, **88**, 7867–7872.

44 Y. Wang, X. Hu, J. Weng, J. Li, Q. Fan, Y. Zhang and D. Ye, *Angew Chem. Int. Ed. Engl.*, 2019, **58**, 4886–4890.

45 H. Shi, R. T. Kwok, J. Liu, B. Xing, B. Z. Tang and B. Liu, *J. Am. Chem. Soc.*, 2012, **134**, 17972–17981.

46 Y. Yuan, R. Zhang, X. Cheng, S. Xu and B. Liu, *Chem. Sci.*, 2016, **7**, 4245–4250.

47 X. Liu, X. Song, D. Luan, B. Hu, K. Xu and B. Tang, *Anal. Chem.*, 2019, **91**, 5994–6002.

48 X. Gao, J. Li, M. Luan, Y. Li, W. Pan, N. Li and B. Tang, *Biosens. Bioelectron.*, 2020, **147**, 111755.

49 B. Bauvois and D. Dauzonne, *Med. Res. Rev.*, 2006, **26**, 88–130.

50 P. Mina-Osorio, *Trends Mol. Med.*, 2008, **14**, 361–371.

51 C. Santiago, G. Mudgal, J. Reguera, R. Recacha, S. Albrecht, L. Enjuanes and J. M. Casasnovas, *Sci. Rep.*, 2017, **7**, 46045.

52 Y. Wang, B. Pang, R. Zhang, Y. Fu and Q. Pang, *Drug Des., Dev. Ther.*, 2019, **13**, 3217–3228.

53 T. Kessler, A. Baumeier, C. Brand, M. Grau, L. Angenendt, S. Harrach, U. Stalmann, L. H. Schmidt, G. Gosheger, J. Hardes, D. Andreou, J. Dreischaluck, G. Lenz, E. Wardelmann, R. M. Mesters, C. Schwoppe, W. E. Berdel, W. Hartmann and C. Schliemann, *Clin. Transl. Oncol.*, 2018, **11**, 1271–1282.

54 Y. Luan and W. Xu, *Curr. Med. Chem.*, 2007, **14**, 639–647.

55 L. Chen, W. Sun, J. Li, Z. Liu, Z. Ma, W. Zhang, L. Du, W. Xu, H. Fang and M. Li, *Org. Biomol. Chem.*, 2013, **11**, 378–382.

56 X. He, Y. Xu, W. Shi and H. Ma, *Anal. Chem.*, 2017, **89**, 3217–3221.

57 X. He, Y. Hu, W. Shi, X. Li and H. Ma, *Chem. Commun.*, 2017, **53**, 9438–9441.

58 H. Li, Q. Yao, W. Sun, K. Shao, Y. Lu, J. Chung, D. Kim, J. Fan, S. Long, J. Du, Y. Li, J. Wang, J. Yoon and X. Peng, *J. Am. Chem. Soc.*, 2020, **142**, 6381–6389.

59 H. Li, Y. Li, Q. Yao, J. Fan, W. Sun, S. Long, K. Shao, J. Du, J. Wang and X. Peng, *Chem. Sci.*, 2019, **10**, 1619–1625.

60 T. Shiomi, V. Lemaitre, J. D'Armiento and Y. Okada, *Pathol. Int.*, 2010, **60**, 477–496.

61 S. T. Alamgeer, U. H. Hasan, A. M. Uttra, S. Qasim, J. Ikram, M. Saleem and Z. R. Niazi, *Phytomedicine*, 2020, **66**, 153134.

62 G. H. Lee, S. W. Jin, S. J. Kim, T. H. Pham, J. H. Choi and H. G. Jeong, *Toxicol. Res.*, 2019, **35**, 93–101.

63 D. E. Lee, M. Y. Chung, T. G. Lim, W. B. Huh, H. J. Lee and K. W. Lee, *J. Food Sci.*, 2013, **78**, H1464–H1469.

64 C. Muvva, S. Patra and S. Venkatesan, *PLoS One*, 2016, **11**, e0159321.

65 C. Gialeli, A. D. Theocharis and N. K. Karamanos, *FEBS J.*, 2011, **278**, 16–27.

66 S. Quintero-Fabian, R. Arreola, E. Becerril-Villanueva, J. C. Torres-Romero, V. Arana-Argaez, J. Lara-Riegos, M. A. Ramirez-Camacho and M. E. Alvarez-Sanchez, *Front. Oncol.*, 2019, **9**, 1370.

67 R. Lee, S. J. Choi, K. C. Moon, J. W. Park, K. Kim, S. Y. Yoon and I. Youn, *ACS Biomater. Sci. Eng.*, 2019, **5**, 3039–3048.

68 A. Lee, S. J. Choi, K. Park, J. W. Park, K. Kim, K. Choi, S. Y. Yoon and I. Youn, *Bioconjugate Chem.*, 2013, **24**, 1068–1074.

69 L. Zhu, Y. Ma, D. O. Kiesewetter, Y. Wang, L. Lang, S. Lee, G. Niu and X. Chen, *ACS Chem. Biol.*, 2014, **9**, 510–516.

70 T. Myochin, K. Hanaoka, S. Iwaki, T. Ueno, T. Komatsu, T. Terai, T. Nagano and Y. Urano, *J. Am. Chem. Soc.*, 2015, **137**, 4759–4765.

71 X. Gao, L. Jiang, B. Hu, F. Kong, X. Liu, K. Xu and B. Tang, *Anal. Chem.*, 2018, **90**, 4719–4724.

72 H. Cheng, S. Y. Li, H. R. Zheng, C. X. Li, B. R. Xie, K. W. Chen, B. Li and X. Z. Zhang, *Anal. Chem.*, 2017, **89**, 4349–4354.

73 L. Yin, H. Sun, H. Zhang, L. He, L. Qiu, J. Lin, H. Xia, Y. Zhang, S. Ji, H. Shi and M. Gao, *J. Am. Chem. Soc.*, 2019, **141**, 3265–3273.

74 Y. Cheng, F. Huang, X. Min, P. Gao, T. Zhang, X. Li, B. Liu, Y. Hong, X. Lou and F. Xia, *Anal. Chem.*, 2016, **88**, 8913–8919.

75 J. Ni, Z. Wu, V. Stoka, J. Meng, Y. Hayashi, C. Peters, H. Qing, V. Turk and H. Nakanishi, *Aging Cell*, 2019, **18**, e12856.

76 S. U. Seo, S. M. Woo, M. W. Kim, H. S. Lee, S. H. Kim, S. C. Kang, E. W. Lee, K. J. Min and T. K. Kwon, *Redox Biol.*, 2020, **30**, 101422.

77 A. M. Szpaderska and A. Frankfater, *Cancer Res.*, 2001, **61**, 3493–3500.

78 V. Turk, V. Stoka, O. Vasiljeva, M. Renko, T. Sun, B. Turk and D. Turk, *Biochim. Biophys. Acta*, 2012, **1824**, 68–88.

79 Y. Wang, J. Li, L. Feng, J. Yu, Y. Zhang, D. Ye and H. Y. Chen, *Anal. Chem.*, 2016, **88**, 12403–12410.

80 M. K. Shim, H. Y. Yoon, J. H. Ryu, H. Koo, S. Lee, J. H. Park, J. H. Kim, S. Lee, M. G. Pomper, I. C. Kwon and K. Kim, *Angew Chem. Int. Ed. Engl.*, 2016, **55**, 14698–14703.

81 X. Chen, D. Lee, S. Yu, G. Kim, S. Lee, Y. Cho, H. Jeong, K. T. Nam and J. Yoon, *Biomaterials*, 2017, **122**, 130–140.

82 Y. Yuan, C. J. Zhang, M. Gao, R. Zhang, B. Z. Tang and B. Liu, *Angew Chem. Int. Ed. Engl.*, 2015, **54**, 1780–1786.

83 M. Rolff, J. Schottenheim, H. Decker and F. Tuczek, *Chem. Soc. Rev.*, 2011, **40**, 4077–4098.

84 R. Freeman, J. Elbaz, R. Gill, M. Zayats and I. Willner, *Chemistry*, 2007, **13**, 7288–7293.

85 M. Perluigi, F. De Marco, C. Foppoli, R. Coccia, C. Blarzino, M. L. Marcante and C. Cini, *Biochem. Biophys. Res. Commun.*, 2003, **305**, 250–256.

86 B. K. Naidu, M. Won, I. Shim, N. Velusamy, Z. Yang, J. Qu, J. S. Kim and S. Bhuniya, *Chem. Commun.*, 2017, **53**, 11213–11216.

87 I. Tessari, M. Bisaglia, F. Valle, B. Samori, E. Bergantino, S. Mammi and L. Bubacco, *J. Biol. Chem.*, 2008, **283**, 16808–16817.

88 K. Cho, C. S. Ryu, S. Jeong and Y. Kim, *Comp. Biochem. Physiol., Part C: Toxicol. Pharmacol.*, 2020, **228**, 108655.

89 J. Zhou, W. Shi, L. Li, Q. Gong, X. Wu, X. Li and H. Ma, *Anal. Chem.*, 2016, **88**, 4557–4564.

90 H. Li, W. Liu, F. Zhang, X. Zhu, L. Huang and H. Zhang, *Anal. Chem.*, 2018, **90**, 855–858.

91 C. Zhan, J. Cheng, B. Li, S. Huang, F. Zeng and S. Wu, *Anal. Chem.*, 2018, **90**, 8807–8815.

92 X. Wu, L. Li, W. Shi, Q. Gong and H. Ma, *Angew Chem. Int. Ed. Engl.*, 2016, **55**, 14728–14732.

93 J. Zhang, Z. Li, X. Tian and N. Ding, *Chem. Commun.*, 2019, **55**, 9463–9466.

94 Z. Li, Y. F. Wang, C. Zeng, L. Hu and X. Liang, *J. Anal. Chem.*, 2018, **90**, 3666–3669.

95 R. Gill, R. Freeman, J. P. Xu, I. Willner, S. Winograd, I. Shweky and U. Banin, *J. Am. Chem. Soc.*, 2006, **128**, 15376–15377.

96 M. Wang, J. L. Xie, J. Li, Y. Y. Fan, X. Deng, H. L. Duan and Z. Q. Zhang, *ACS Sens.*, 2020, **5**, 1634–1640.

97 Y. Chen, *Anal. Biochem.*, 2020, **594**, 113614.

98 X. Yan, H. Li, W. Zheng and X. Su, *Anal. Chem.*, 2015, **87**, 8904–8909.

99 M. Peng, Y. Wang, Q. Fu, F. Sun, N. Na and J. Ouyang, *Anal. Chem.*, 2018, **90**, 6206–6213.

100 T. I. Kim, J. Park, S. Park, Y. Choi and Y. Kim, *Chem. Commun.*, 2011, **47**, 12640–12642.

101 R. Drozdz, C. Parmentier, H. Hachad, P. Leroy, G. Siest and M. Wellman, *Free Radic. Biol. Med.*, 1998, **25**, 786–792.

102 M. J. Accaoui, M. Enoiu, M. Mergny, C. Masson, S. Dominici, M. Wellman and A. Visvikis, *Biochem. Biophys. Res. Commun.*, 2000, **276**, 1062–1067.

103 M. W. Lieberman, A. L. Wiseman, Z. Z. Shi, B. Z. Carter, R. Barrios, C. N. Ou, P. Chevez-Barrios, Y. Wang, G. M. Habib, J. C. Goodman, S. L. Huang, R. M. Lebovitz and M. M. Matzuk, *Proc. Natl. Acad. Sci. U. S. A.*, 1996, **93**, 7923–7926.

104 S. S. Terzyan, A. W. Burgett, A. Heroux, C. A. Smith, B. H. Mooers and M. H. Hanigan, *J. Biol. Chem.*, 2015, **290**, 17576–17586.

105 M. B. West, Y. Chen, S. Wickham, A. Heroux, K. Cahill, M. H. Hanigan and B. H. Mooers, *J. Biol. Chem.*, 2013, **288**, 31902–31913.

106 A. Paolicchi, A. Pompella, P. Tonarelli, A. Gadducci, A. R. Genazzani, F. Zunino, G. Pratesi and R. Tongiani, *Anticancer Res.*, 1996, **16**, 3053–3058.

107 H. Ma, L. Zhang, B. Tang, Y. Wang, R. Chen, B. Zhang, Y. Chen, N. Ge, Y. Wang, Y. Gan, S. Ye and Z. Ren, *Ann. Surg Oncol.*, 2014, **21**, 3084–3089.

108 S. Park, D. J. Bae, Y. M. Ryu, S. Y. Kim, S. J. Myung and H. J. Kim, *Chem. Commun.*, 2016, **52**, 10400–10402.

109 X. Zhou, Y. Liu, Q. Liu, L. Yan, M. Xue, W. Yuan, M. Shi, W. Feng, C. Xu and F. Li, *Theranostics*, 2019, **9**, 4597–4607.

110 J. Ou-Yang, Y. Li, W. L. Jiang, S. Y. He, H. W. Liu and C. Y. Li, *Anal. Chem.*, 2019, **91**, 1056–1063.

111 Z. Luo, Z. Huang, K. Li, Y. Sun, J. Lin, D. Ye and H. Y. Chen, *Anal. Chem.*, 2018, **90**, 2875–2883.

112 F. Liu, Z. Wang, W. Wang, J. G. Luo and L. Kong, *Anal. Chem.*, 2018, **90**, 7467–7473.

113 H. Zhang, K. Wang, X. Xuan, Q. Lv, Y. Nie and H. Guo, *Chem. Commun.*, 2016, **52**, 6308–6311.

114 L. Li, W. Shi, Z. Wang, Q. Gong and H. Ma, *Anal. Chem.*, 2015, **87**, 8353–8359.

115 J. Liu, S. Zhang, B. Zhao, C. Shen, X. Zhang and G. Yang, *Biosens. Bioelectron.*, 2019, **142**, 111497.

116 T. Fujii, M. Kamiya and Y. Urano, *Bioconjugate Chem.*, 2014, **25**, 1838–1846.

117 H. Tong, Y. Zheng, L. Zhou, X. Li, R. Qian, R. Wang, J. Zhao, K. Lou and W. Wang, *Anal. Chem.*, 2016, **88**, 10816–10820.

118 H. Li, Q. Yao, F. Xu, N. Xu, R. Duan, S. Long, J. Fan, J. Du, J. Wang and X. Peng, *Biomaterials*, 2018, **179**, 1–14.

119 Y. Urano, M. Sakabe, N. Kosaka, M. Ogawa, M. Mitsunaga, D. Asanuma, M. Kamiya, M. R. Young, T. Nagano, P. L. Choyke and H. Kobayashi, *Sci. Transl. Med.*, 2011, **3**, 110ra119.

120 R. J. Iwatate, M. Kamiya and Y. Urano, *Chemistry*, 2016, **22**, 1696–1703.

121 R. J. Iwatate, M. Kamiya, K. Umezawa, H. Kashima, M. Nakadate, R. Kojima and Y. Urano, *Bioconjugate Chem.*, 2018, **29**, 241–244.

122 Q. Husain, *Crit. Rev. Biotechnol.*, 2010, **30**, 41–62.

123 G. P. Dimri, X. Lee, G. Basile, M. Acosta, G. Scott, C. Roskelley, E. E. Medrano, M. Linskens, I. Rubelj, O. Pereira-Smith and A. Et, *Proc. Natl. Acad. Sci. U. S. A.*, 1995, **92**, 9363–9367.

124 J. Zhang, P. Cheng and K. Pu, *Bioconjugate Chem.*, 2019, **30**, 2089–2101.

125 M. Kamiya, D. Asanuma, E. Kuranaga, A. Takeishi, M. Sakabe, M. Miura, T. Nagano and Y. Urano, *J. Am. Chem. Soc.*, 2011, **133**, 12960–12963.

126 D. Asanuma, M. Sakabe, M. Kamiya, K. Yamamoto, J. Hiratake, M. Ogawa, N. Kosaka, P. L. Choyke, T. Nagano, H. Kobayashi and Y. Urano, *Nat. Commun.*, 2015, **6**, 6463.

127 X. Kong, M. Li, B. Dong, Y. Yin, W. Song and W. Lin, *Anal. Chem.*, 2019, **91**, 15591–15598.

128 K. Gu, Y. Xu, H. Li, Z. Guo, S. Zhu, S. Zhu, P. Shi, T. D. James, H. Tian and W. H. Zhu, *J. Am. Chem. Soc.*, 2016, **138**, 5334–5340.

129 E. J. Kim, R. Kumar, A. Sharma, B. Yoon, H. M. Kim, H. Lee, K. S. Hong and J. S. Kim, *Biomaterials*, 2017, **122**, 83–90.

130 X. Li, Y. Pan, H. Chen, Y. Duan, S. Zhou, W. Wu, S. Wang and B. Liu, *Anal. Chem.*, 2020, **92**, 5772–5779.

131 J. A. Chen, H. Pan, Z. Wang, J. Gao, J. Tan, Z. Ouyang, W. Guo and X. Gu, *Chem. Commun.*, 2020, **56**, 2731–2734.

132 G. Jiang, G. Zeng, W. Zhu, Y. Li, X. Dong, G. Zhang, X. Fan, J. Wang, Y. Wu and B. Z. Tang, *Chem. Commun.*, 2017, **53**, 4505–4508.

133 Y. Kayama, U. Raaz, A. Jagger, M. Adam, I. N. Schellinger, M. Sakamoto, H. Suzuki, K. Toyama, J. M. Spin and P. S. Tsao, *Int. J. Mol. Sci.*, 2015, **16**, 25234–25263.

134 H. Pei, Y. Yang, H. Zhao, X. Li, D. Yang, D. Li and Y. Yang, *Oxid. Med. Cell. Longevity*, 2016, **2016**, 5470457.

135 C. A. Lygate, S. Bohl, H. M. Ten, K. M. Faller, P. J. Ostrowski, S. Zervou, D. J. Medway, D. Aksentijevic, L. Sebag-Montefiore, J. Wallis, K. Clarke, H. Watkins, J. E. Schneider and S. Neubauer, *Cardiovasc. Res.*, 2012, **96**, 466–475.

136 T. Zang, Y. Xie, S. Su, F. Liu, Q. Chen, J. Jing, R. Zhang, G. Niu and X. Zhang, *Angew Chem. Int. Ed. Engl.*, 2020, **59**, 10003–10007.

137 L. Zhang, D. Duan, Y. Liu, C. Ge, X. Cui, J. Sun and J. Fang, *J. Am. Chem. Soc.*, 2014, **136**, 226–233.

138 H. Ma, J. Zhang, Z. Zhang, Y. Liu and J. Fang, *Chem. Commun.*, 2016, **52**, 12060–12063.

139 X. Li, B. Zhang, C. Yan, J. Li, S. Wang, X. Wei, X. Jiang, P. Zhou and J. Fang, *Nat. Commun.*, 2019, **10**, 2745.

140 M. Hamer and Y. Chida, *Psychol. Med.*, 2009, **39**, 3–11.

141 H. Quan, E. Koltai, K. Suzuki, A. J. Aguiar, R. Pinho, I. Boldogh, I. Berkes and Z. Radak, *Biochim. Biophys. Acta, Mol. Basis Dis.*, 2020, **1866**, 165778.

142 Z. Liu, T. Zhou, A. C. Ziegler, P. Dimitrion and L. Zuo, *Oxid. Med. Cell. Longevity*, 2017, **2017**, 2525967.

143 H. Fu, M. Cui, P. Tu, Z. Pan and B. Liu, *Chem. Commun.*, 2014, **50**, 11875–11878.

144 X. Zhang, Y. Tian, Z. Li, X. Tian, H. Sun, H. Liu, A. Moore and C. Ran, *J. Am. Chem. Soc.*, 2013, **135**, 16397–16409.

145 C. H. Heo, K. H. Kim, H. J. Kim, S. H. Baik, H. Song, Y. S. Kim, J. Lee, I. Mook-jung and H. M. Kim, *Chem. Commun.*, 2013, **49**, 1303–1305.

146 G. Lv, A. Sun, P. Wei, N. Zhang, H. Lan and T. Yi, *Chem. Commun.*, 2016, **52**, 8865–8868.

147 W. Fu, C. Yan, Z. Guo, J. Zhang, H. Zhang, H. Tian and W. H. Zhu, *J. Am. Chem. Soc.*, 2019, **141**, 3171–3177.

148 J. D. Zhang, J. Mei, X. L. Hu, X. P. He and H. Tian, *Small*, 2016, **12**, 6562–6567.

149 M. Goedert and M. G. Spillantini, *Science*, 2006, **314**, 777–781.

150 W. H. Stoothoff and G. V. Johnson, *Biochim. Biophys. Acta*, 2005, **1739**, 280–297.

151 N. Esteras, J. D. Rohrer, J. Hardy, S. Wray and A. Y. Abramov, *Redox Biol.*, 2017, **12**, 410–422.

152 J. Gu, U. R. Anumala, H. R. Heyny-von, J. Holzer, V. Goetschy-Meyer, G. Mall, I. Hilger, C. Czech and B. Schmidt, *ChemMedChem*, 2013, **8**, 891–897.

153 S. Lim, M. M. Haque, D. Su, D. Kim, J. S. Lee, Y. T. Chang and Y. K. Kim, *Chem. Commun.*, 2017, **53**, 1607–1610.

154 Y. Seo, K. S. Park, T. Ha, M. K. Kim, Y. J. Hwang, J. Lee, H. Ryu, H. Choo and Y. Chong, *ACS Chem. Neurosci.*, 2016, **7**, 1474–1481.

155 K. S. Park, Y. Seo, M. K. Kim, K. Kim, Y. K. Kim, H. Choo and Y. Chong, *Org. Biomol. Chem.*, 2015, **13**, 11194–11199.

156 E. Vandermarliere, B. Ghesquiere, V. Jonckheere, K. Gevaert and L. Martens, *Proteomics*, 2014, **14**, 1990–1998.

157 L. Lai, J. Sun, S. Tarafdar, C. Liu, E. Murphy, G. Kim and R. L. Levine, *Free Radic. Biol. Med.*, 2019, **145**, 374–384.

158 M. L. Circu and T. Y. Aw, *Free Radic. Biol. Med.*, 2010, **48**, 749–762.

159 X. Wu, W. Shi, X. Li and H. Ma, *Angew Chem. Int. Ed. Engl.*, 2017, **56**, 15319–15323.

160 W. Y. Kim, M. Won, A. Salimi, A. Sharma, J. H. Lim, S. H. Kwon, J. Y. Jeon, J. Y. Lee and J. S. Kim, *Chem. Commun.*, 2019, **55**, 13267–13270.

161 L. Li, C. W. Zhang, G. Y. Chen, B. Zhu, C. Chai, Q. H. Xu, E. K. Tan, Q. Zhu, K. L. Lim and S. Q. Yao, *Nat. Commun.*, 2014, **5**, 3276.

162 L. Li, C. W. Zhang, J. Ge, L. Qian, B. H. Chai, Q. Zhu, J. S. Lee, K. L. Lim and S. Q. Yao, *Angew Chem. Int. Ed. Engl.*, 2015, **54**, 10821–10825.

163 H. Fang, H. Zhang, L. Li, Y. Ni, R. Shi, Z. Li, X. Yang, B. Ma, C. Zhang, Q. Wu, C. Yu, N. Yang, S. Q. Yao and W. Huang, *Angew Chem. Int. Ed. Engl.*, 2020, **59**, 7536–7541.

164 Z. M. Yang, Q. Y. Mo, J. M. He, D. L. Mo, J. Li, H. Chen, S. L. Zhao and J. K. Qin, *ACS Sens.*, 2020, **5**, 943–951.

165 R. Wang, X. Han, J. You, F. Yu and L. Chen, *Anal. Chem.*, 2018, **90**, 4054–4061.

166 Y. Liu, L. Teng, C. Xu, H. W. Liu, S. Xu, H. Guo, L. Yuan and X. B. Zhang, *Chem. Sci.*, 2019, **10**, 10931–10936.

167 W. Li, W. Li, Y. Hu, Y. Xia, Q. Shen, Z. Nie, Y. Huang and S. Yao, *Biosens. Bioelectron.*, 2013, **47**, 345–349.

168 X. Wang, P. Li, Q. Ding, C. Wu, W. Zhang and B. Tang, *J. Am. Chem. Soc.*, 2019, **141**, 2061–2068.

169 J. Ma, T. Si, C. Yan, Y. Li, Q. Li, X. Lu and Y. Guo, *ACS Sens.*, 2020, **5**, 83–92.

170 Y. Chen, W. Liu, B. Zhang, Z. Suo, F. Xing and L. Feng, *Anal. Biochem.*, 2020, **607**, 113835.

171 X. Xu, Y. Cen, G. Xu, F. Wei, M. Shi and Q. Hu, *Biosens. Bioelectron.*, 2019, **131**, 232–236.

172 Y. Zhang, Y. Cai, Z. Qi, L. Lu and Y. Qian, *Anal. Chem.*, 2013, **85**, 8455–8461.

173 X. Xu, Y. Cen, G. Xu, F. Wei, M. Shi and Q. Hu, *Biosens. Bioelectron.*, 2019, **131**, 232–236.

174 K. Kis, X. Liu and J. S. Hagood, *Expert Rev. Mol. Med.*, 2011, **13**, e27.

175 R. Kramann, D. P. DiRocco and B. D. Humphreys, *J. Pathol.*, 2013, **231**, 273–289.

176 M. T. Levy, G. W. McCaughan, C. A. Abbott, J. E. Park, A. M. Cunningham, E. Muller, W. J. Rettig and M. D. Gorrell, *Hepatology*, 1999, **29**, 1768–1778.

177 A. Simkova, P. Busek, A. Sedo and J. Konvalinka, *Biochim. Biophys. Acta, Proteins Proteomics*, 2020, **1868**, 140409.

178 N. Sampson, E. Brunner, A. Weber, M. Puhr, G. Schafer, C. Szyndralewiez and H. Klocker, *Int. J. Cancer*, 2018, **143**, 383–395.

179 J. Xing, Q. Gong, R. Zou, Z. Li, Y. Xia, Z. Yu, Y. Ye, L. Xiang and A. Wu, *J. Mater. Chem. B*, 2018, **6**, 1449–1451.

180 A. Simkova, P. Busek, A. Sedo and J. Konvalinka, *Biochim. Biophys. Acta, Proteins Proteomics*, 2020, **1868**, 140409.

181 Y. Lin, Z. Ma, Z. Li, Y. Gao, X. Qin, Z. Zhang, G. Wang, L. Du and M. Li, *Anal. Chem.*, 2019, **91**, 14873–14878.

182 Q. Miao, D. C. Yeo, C. Wiraja, J. Zhang, X. Ning, C. Xu and K. Pu, *Angew Chem. Int. Ed. Engl.*, 2018, **57**, 1256–1260.

183 J. Xing, Q. Gong, R. Zou, Z. Li, Y. Xia, Z. Yu, Y. Ye, L. Xiang and A. Wu, *J. Mater. Chem. B*, 2018, **6**, 1449–1451.

184 J. Li, K. Chen, H. Liu, K. Cheng, M. Yang, J. Zhang, J. D. Cheng, Y. Zhang and Z. Cheng, *Bioconjugate Chem.*, 2012, **23**, 1704–1711.

185 H. Raza, M. A. Robin, J. K. Fang and N. G. Avadhani, *Biochem. J.*, 2002, **366**, 45–55.

186 A. Oakley, *Drug Metab. Rev.*, 2011, **43**, 138–151.

187 Y. Fujikawa, Y. Urano, T. Komatsu, K. Hanaoka, H. Kojima, T. Terai, H. Inoue and T. Nagano, *J. Am. Chem. Soc.*, 2008, **130**, 14533–14543.

188 N. He, S. Bai, Y. Huang, Y. Xing, L. Chen, F. Yu and C. Lv, *Anal. Chem.*, 2019, **91**, 5424–5432.

189 F. Martinon, *Eur. J. Immunol.*, 2010, **40**, 616–619.

190 K. J. Cho, J. M. Seo and J. H. Kim, *Mol. Cells*, 2011, **32**, 1–5.

191 X. Jiang, L. Zhou, D. Wei, H. Meng, Y. Liu and L. Lai, *Bioorg. Med. Chem. Lett.*, 2008, **18**, 6549–6552.

192 H. Wang, K. Xue, P. Li, Y. Yang, Z. He, W. Zhang, W. Zhang and B. Tang, *Anal. Chem.*, 2018, **90**, 6020–6027.

193 H. Wang, K. Xue, Z. Duan, Y. Yang, Z. He, C. Wu, W. Zhang, W. Zhang, P. Li and B. Tang, *Sens. Actuators, B*, 2019, **286**, 243–249.

194 Q. Sun, J. Li, W. N. Liu, Q. J. Dong, W. C. Yang and G. F. Yang, *Anal. Chem.*, 2013, **85**, 11304–11311.

195 S. Y. Liu, H. Xiong, R. R. Li, W. C. Yang and G. F. Yang, *Anal. Chem.*, 2019, **91**, 3877–3884.

196 J. A. Chen, H. Pan, Z. Wang, J. Gao, J. Tan, Z. Ouyang, W. Guo and X. Gu, *Chem. Commun.*, 2020, **56**, 2731–2734.

197 X. Jie, M. Wu, H. Yang and W. Wei, *Anal. Chem.*, 2019, **91**, 13174–13182.

198 Y. Cheng, F. Huang, X. Min, P. Gao, T. Zhang, X. Li, B. Liu, Y. Hong, X. Lou and F. Xia, *Anal. Chem.*, 2016, **88**, 8913–8919.